Geothermics 140 (2026) 103698

Contents lists available at ScienceDirect

Geothermics

journal homepage: www.elsevier.com/locate/geothermics

Solar-assisted borehole thermal energy storage coupled with heat pump for livestock buildings: results from a full-scale installation

Francesco Tinti [a,*], Carlos Alejandro Perez Garcia [b], Panteleimon Bakalis [c], Iván Acosta-Pazmiño [d], Stefano Benni [b]

[a] Department of Civil, Chemical, Environmental, and Materials Engineering, University of Bologna, Via Terracini, 28, Bologna, 40131, Italy
[b] Department of Agricultural and Food Sciences, University of Bologna, Viale Fanin 44, 40127, Bologna, Italy
[c] Psyctotherm G. Ligeros and Sia OE, Vasiladiou 6, Piraeus, 18540, Greece
[d] MG Sustainable Engineering AB, Stationsgatan 23, Uppsala, 75340, Sweden

ARTICLE INFO

Keywords:
Borehole thermal energy storage
Dual source heat pump
Geothermal energy for livestock

ABSTRACT

Livestock farming is an energy-intensive sector of agriculture and a significant contributor to greenhouse gas emissions. This study presents the first-year operational results of an integrated renewable energy system combining photovoltaic–thermal (PVT) collectors, borehole thermal energy storage (BTES), and a dual-source heat pump (DSHP) for space heating in a commercial swine nursery building.

The BTES is based on a novel "double-circuit" configuration, allowing the exploitation of solar energy during mid-season and summer periods, while ensuring reliable heat supply during winter peak loads.

A monitoring system, including dedicated piezometers aligned with groundwater flow, was implemented to continuously record environmental conditions inside the building, system operating parameters, energy flows, and subsurface temperature variations. During the first year, the system met the heating demand of the nursery barn, achieving an overall Seasonal Performance Factor (SPF) of 3.78. Approximately 54% of the heat pump operation occurred in hybrid ground–air mode, 38% in ground-only mode, and only 7% in air-only mode, demonstrating the effectiveness of the strategy in balancing performance and resource preservation. The installed system employed only 240 m of borehole heat exchangers, compared to an estimated 640 m required for conventional systems delivering comparable thermal performance. Subsurface monitoring confirmed that the thermal impact on the aquifer was limited and remained well below regulatory thresholds.

The results demonstrate that solar-assisted BTES coupled with a DSHP represents a technically effective, energy-efficient, and environmentally compatible solution for decarbonising heating in livestock buildings, particularly in rural areas with available land and suitable hydrogeological conditions.

1. Introduction

Heating, ventilation, and air conditioning are commonly applied for controlling the environmental parameters in livestock farms and intensive crop production facilities. Traditional systems often rely on lpg and natural gas, leading to significant greenhouse gas emissions. Recent studies report that such sectors account for 10–15 % of the whole global emissions (FAO, 2019); however, the exact quantification is object of debate among researchers (Nugrahaeningtyas et al., 2024; He, et al., 2023). These numbers have raised concerns about the sustainability especially of intensive livestock farming (Tyris et al., 2022). Many technological advancements have been conducted in recent years; for instance, radiant heating and heat recovery ventilation have been successfully applied (Deeken et al., 2023). On the other hand, renewable energy sources, such as solar panels for both electrical and thermal production, have proved to be easily installed on the roofs of the production's facilities, to enhance sustainability (Pal et al., 2025)

Moreover, it is worth noticing that livestock farms and crop production facilities, as well as companies located in rural areas more generally, typically have extensive land availability that can be exploited for shallow geothermal energy systems based on borehole heat exchangers (BHEs), generally connected to ground source heat pumps (GSHP). These systems are considered environmentally friendly due to

* Corresponding author.
E-mail addresses: francesco.tinti@unibo.it (F. Tinti), carlos.perezgarcia2@unibo.it (C.A. Perez Garcia), pbakalis@psyctotherm.gr (P. Bakalis), ivan@mgsust.com (I. Acosta-Pazmiño), stefano.benni@unibo.it (S. Benni).

https://doi.org/10.1016/j.geothermics.2026.103698
Received 2 February 2026; Received in revised form 25 March 2026; Accepted 19 April 2026
0375-6505/© 2026 The Author(s). Published by Elsevier Ltd. This is an open access article under the CC BY license (http://creativecommons.org/licenses/by/4.0/).

Nomenclature

Acronyms

ASHP	Air Source Heat Pump
BHE	Borehole Heat Exchanger
BTES	Borehole Thermal Energy Storage
COP	Coefficient of Performance
DSHP	Dual Source Heat Pump
GSHP	Ground Source Heat Pump
LPG	Liquified Petroleum Gas
MPF	Monthly Performance Factor
SPF	Seasonal Performance Factor
TRT	Thermal Response Test
PV	Photovoltaic Solar Panel
PVT	Photovoltaic-Thermal Solar Panel
UTES	Underground Energy Storage

Subscripts

ambient	ambient source
air	air source
building	building end-user
effective	practical
ground	ground source
i	step
ideal	theoretical
in	inlet
out	outlet
m	mean
mod	modified
nat	natural
solar	solar source
T_0	minimum temperature

Symbols

α	Thermal diffusivity
c	Specific heat
E	Thermal energy
L	Electric energy
H	Heat
P	Absorbed Power
Q	Flow
ρ	Density
t	Time
T	Temperature
V	Volume

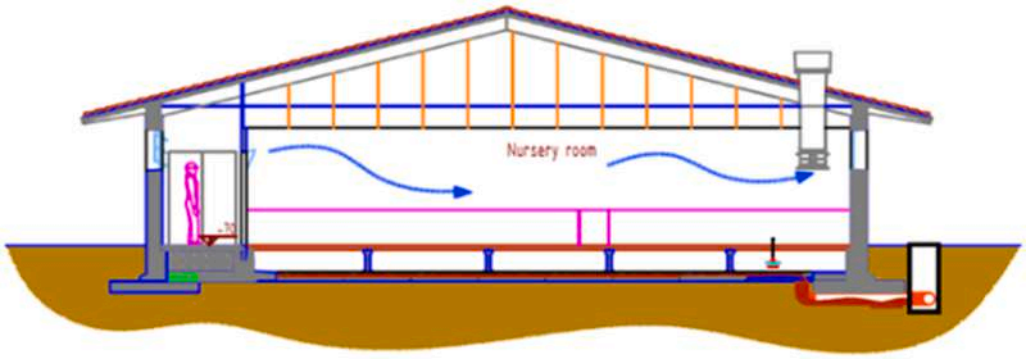

Fig. 1. View of a nursery room, heated mainly by the radiant heat from the hallway.

their limited impact on aquifers (Barbaresi et al., 2020). The extraction of the required thermal energy from the subsurface using geothermal heat exchangers (GHEs) generally demands large volumes of subsoil (Focaccia et al., 2016). Because increasing the installation depth of GHEs entails high costs, a common design strategy consists of replicating and hydraulically connecting multiple exchangers in series or in parallel, resulting in significant spatial requirements (Giambastiani et al., 2014). Consequently, agricultural and farming areas are particularly well suited for the deployment of such systems (Alberti et al., 2018).

In addition, vertical GHEs, namely borehole heat exchangers, can also be employed as underground thermal energy storage (UTES) systems by injecting surplus or waste heat into the subsurface, thereby artificially increasing the temperature of the aquifers (Brown et al., 2024). Following the charging phase during the summer, the stored thermal energy can be recovered in the subsequent winter season by reversing the flow direction within the BHEs, thus meeting the thermal demands of farming facilities (Sadeghi et al., 2024). Among the available energy sources, solar thermal energy is considered one of the most promising options for UTES applications, owing to its pronounced temporal mismatch with building heating requirements (Xiuting et al., 2024).

The main barrier to the wide installation of GHE and UTES system resides in the high installation cost, compared to fossil fuel boilers but also to alternative renewable energy sources, including solar. This has been object of debate for decades among researchers, institutions, companies and policy makers (Chiavetta et al., 2011; Nitkiewicz and Sekret, 2014; Emmi et al., 2017; Tiktas and Hepbasli, 2026). Even if the use of fossil fuels is generally cheaper in urban areas compared to GSHPs, the specific nature of livestock farms and crop production facilities, and their localization in the rural environment, deserve some additional considerations: The production facilities are generally not connected to the natural gas grid; therefore, a specific management of the fuel supply must be considered, which sums to the usual business of the farms;

- Each facility must respect rigid environmental and health regulations, in order to not affect the productions, and subsequently be subjected to sanctions. In such context, the presence of liquified petroleum gas (LPG) or diesel fuel tanks is a potential source of pollution and contamination, and therefore of risk;
- The fluctuating behavior of fossil fuel prices can affect the various businesses of the farms, which instead aim to keep the production costs as constant as possible, in order to always be attractive for the market.

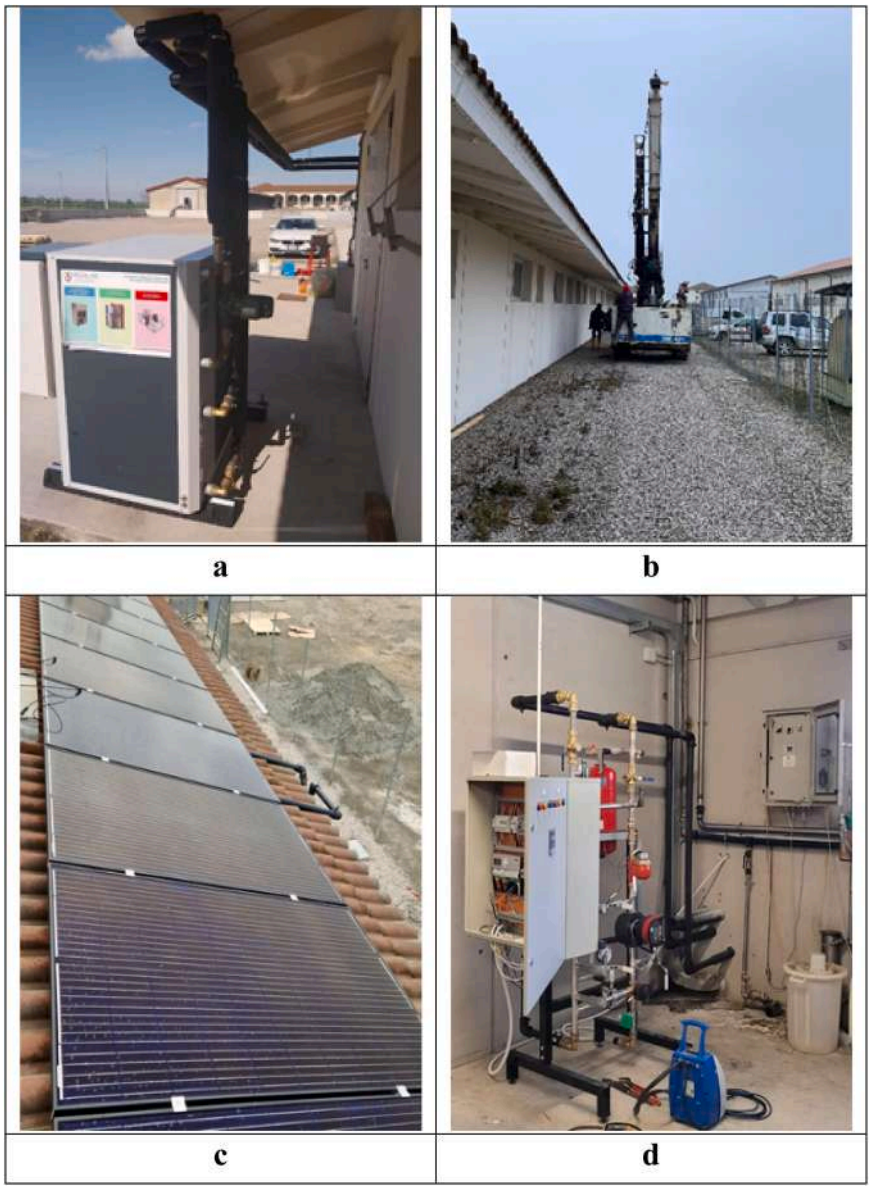

Fig. 2. System's components: dual source heat pump (a), borehole thermal energy storage field installation in the courtyard (b), thermophotovoltaic system on the roof (c), solar central station (d).

Relating to solar energy, the photovoltaic (PV) panels are widespread in the sector, used to cover the electricity consumptions of the farms. The match between electric production and air conditioning of the farms facilitates their introduction, while mismatches are increasingly covered by electric batteries (Li et al., 2026). An indirect benefit of installing PV in farms is the increased economic convenience of electrification of tractors and forklifts, aiming to a cleaner food production (Lombardi and Berni, 2021). Due to such advantages, many subsidies currently exist at local and national levels to increase the use of PV in the rural sector (Tamborrino et al., 2026). With regard to solar thermal panels, their use in the farms instead remains limited due to the mismatch between energy request and production (Ramadhani et al., 2025). To tackle such limitation, an effective solution is the proper installation of long-term thermal energy storage system, among which the UTES proved to have major potential (Naranjo-Mendoza et al., 2019; Fadzlin et al., 2025).

In such context, the integration of solar electric and thermal energy systems with BHEs in agricultural buildings has therefore been the subject of extensive research, with greenhouses being identified as a particularly relevant application, especially with regard to heating demands (Dhaidaan et al., 2024). Several studies have assessed the enhancement of system efficiency achieved through the integration of geothermal and photovoltaic technologies for greenhouse heating in cold climatic regions (Ghiasi et al., 2025). The results of these investigations confirmed that hybrid renewable energy systems play a key role in achieving sustainable heating solutions, enabling the maintenance of indoor temperatures within the optimal range of 19–24 °C throughout the year. In this context, the performance of heat pumps is a critical factor for greenhouse applications. This aspect has been further explored by various authors, who focused on the development of design and simulation models for solar photovoltaic–driven greenhouses (Asgari et al., 2025). Their findings demonstrated that low-carbon heating in greenhouses can be effectively achieved by employing heat pump systems powered by cost-effective renewable energy sources, such as photovoltaic installations.

The integration of solar energy systems, particularly photovoltaic–thermal (PVT) technologies, with geothermal sources has been extensively investigated in the scientific literature, with specific

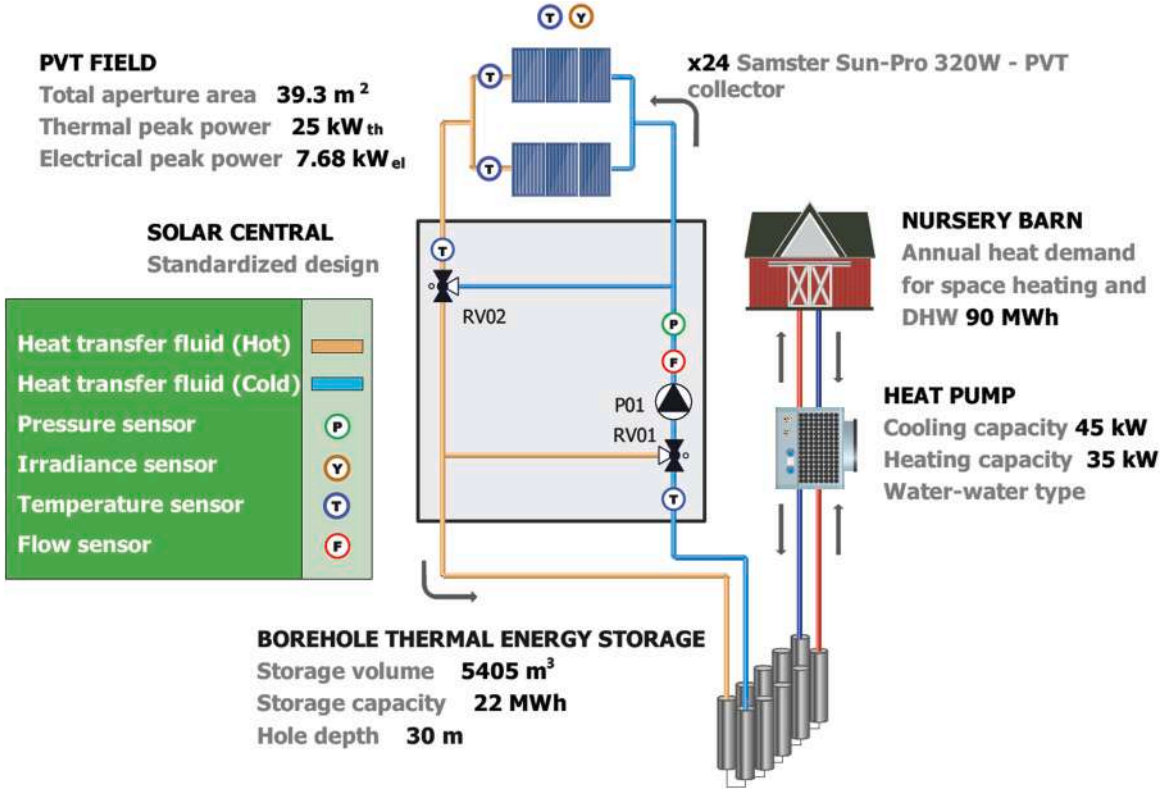

Fig. 3. Simplified schematic of the integrated system, controlled by the solar station (heat injection phase) and by the DSHP (heat extraction phase), and monitored by PLEGMA Labs.

emphasis on animal production and livestock farming applications (Qamar et al., 2026). Within this framework, studies conducted under the European RES4LIVE project assessed the renewable energy source potential of livestock farms through the adoption of these integrated technologies (Benni et al., 2023; Tyris et al., 2022). In particular, the performance of solar PVT systems in livestock facilities was analysed, providing valuable insights into meeting the energy demands of cattle (Hosouli et al., 2023) and swine farms (Murali et al., 2024), while accounting for the opportunities offered by geothermal heat exchange for seasonal thermal energy storage.

The potential of geothermal storage was further explored through an experimental approach involving its integration with a dual-source heat pump (DSHP) system (Tinti et al., 2023). In this context, the execution of Thermal Response Tests (TRTs) at different depths proved to be essential for validating the performance of borehole heat exchangers (BHEs) (Tinti, 2022). Based on these activities, a step-by-step methodology was developed and tested to characterize the shallow geothermal reservoir and to define the optimal design of a Borehole Thermal Energy Storage (BTES) system. The results highlighted that the identification of an effective solution requires the acquisition of detailed geological and hydrogeological information, as well as an accurate characterization of the ground's thermophysical properties.

Preliminary performance assessments carried out over limited time periods confirmed the validity of the proposed approach (Benni et al., 2025). Overall, the research project demonstrated that effective control of environmental conditions in livestock barns can be achieved through the implementation of smart heating systems powered by renewable energy sources (Benni et al., 2024).

2. Theoretical background

Ground temperature T_{ground}, dampening with depth in shallow subsoil, follows Eq. (1).

$$T_{ground}(d,t) = T_m - A \cdot exp\left[-d\cdot\sqrt{\frac{\pi}{365\cdot\alpha_{ground}}}\right]\cdot cos\left[\frac{2\cdot\pi}{365}\cdot\left(t - t_{T_0} - \frac{d}{2}\right)\cdot\sqrt{\frac{365}{\pi\cdot\alpha_{ground}}}\right] \quad (1)$$

Where T_{ground} is the ground temperature, varying with depth d and time t, T_m is the mean of seasonal air temperature, A is the temperature amplitude, α_{ground} is the ground thermal diffusivity and t_{To} is time of minimum air temperature.

The ground temperature inside the volume of the BTES is locally modified according to the energy injected and extracted through the BHEs. Due to the geometry of BTES, the groundwater conditions and the effective heat injection and extraction cycles, some areas (usually the central volume of the BTES, the so-called "thermal core") keep their modifications along the whole season; the real seasonal thermal energy storage involves is delimited by such volumes.

The energy provided by the BTES to the DSHP E_{BTES} is based on Eq. (2).

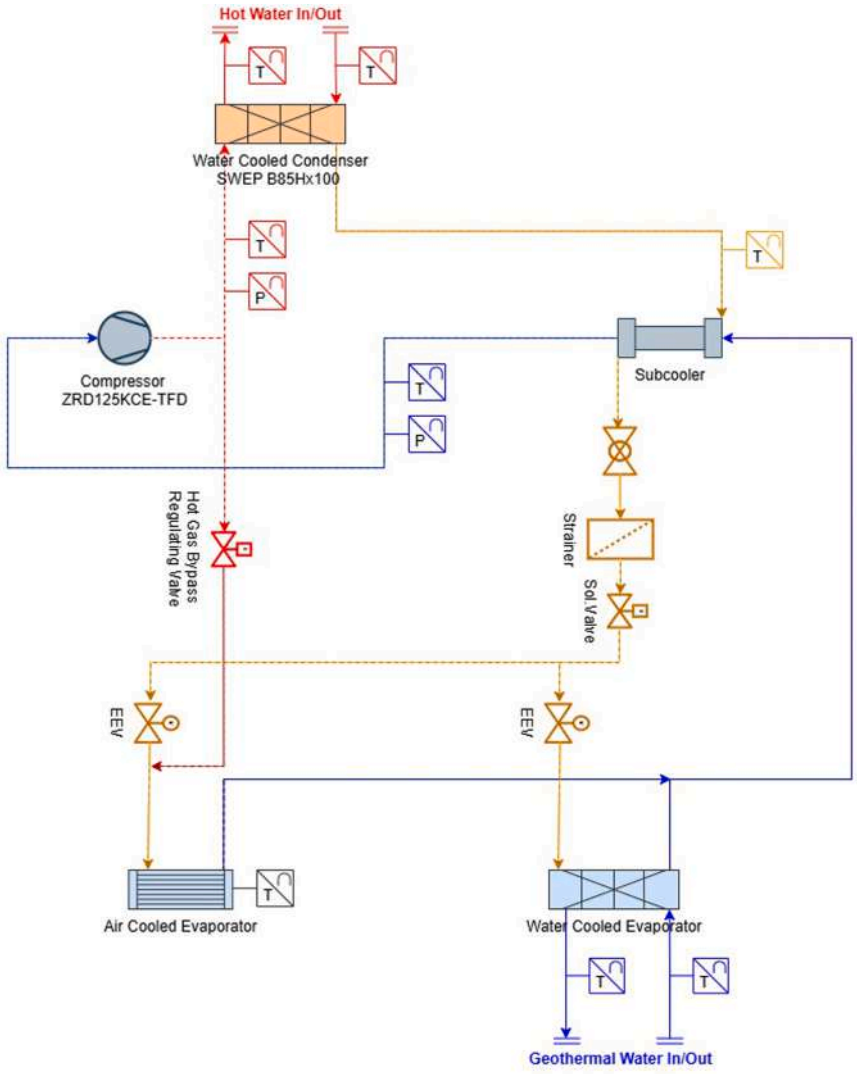

Fig. 4. Detailed schematic of the DSHP components, with connection to the building (hot water in/out) and the borehole thermal energy storage (geothermal water in/out).

$$E_{BTES} = \sum_{i=1}^{n} \left(T_{in,BTES,i} - T_{out,BTES,i}\right) \cdot Q_{BTES,i} \cdot c_{BTES} \cdot \rho_{BTES} \cdot (t_i - t_{i-1}) \quad (2)$$

Where ($T_{in,BTES,i}$-$T_{out,BTES,i}$) is the fluid temperature difference exchanged in the evaporator at the time step i; $Q_{BTES,i}$ is the fluid flow from the BTES to the DSHP; c_{BTES} is the specific heat of the fluid circulating in the BTES, ρ_{BTES} is the density of the fluid circulating in the BTES and (t_i-t_{i-1}) is the reference period step for the energy calculation.

On the condenser side, the energy provided by the DSHP to the building (from both geothermal and air source) $E_{building}$ is based on Eq. (3).

$$E_{building} = \sum_{i=1}^{n} \left(T_{out,building,i} - T_{in,building,i}\right) \cdot Q_{building,i} \cdot c_{building} \cdot \rho_{building} \cdot (t_i - t_{i-1}) \quad (3)$$

Where ($T_{in,building,i}$-$T_{out,building,i}$) is the fluid temperature difference exchanged in the condenser at the time step i (K); $Q_{building,i}$ is the fluid flow towards the building from the DSHP ($m^3 \cdot s^{-1}$); $c_{building}$ is the specific heat of the fluid circulating in the building ($J \cdot kg^{-1} \cdot K^{-1}$); $\rho_{building}$ is the density of the fluid circulating in the building ($kg \cdot m^{-3}$); and (t_i-t_{i-1}) is the reference period step for the energy calculation (s).

Referring to the injected energy in the BTES from the solar station E_{solar}, the equation is the following:

$$E_{solar} = \sum_{i=1}^{n} \left(T_{in,solar,i} - T_{out,solar,i}\right) \cdot Q_{solar,i} \cdot c_{solar} \cdot \rho_{solar} \cdot (t_i - t_{i-1}) \quad (4)$$

Where ($T_{in,solar,i}$-$T_{out,solar,i}$) is the fluid temperature difference exchanged in the BTES at the time step i (K); $Q_{solar,i}$ is the fluid flow towards the BTES from the PVT; $c_{p\ solar}$ is the specific heat of the fluid circulating in the BTES, ρ_{solar} is the density of the fluid circulating in the BTES and (t_i-t_{i-1}) is the reference period step for the energy calculation.

Due to the heat transfer effects in the ground, not all the injected energy is stored in the BTES, but some is transferred under the form of thermal plume. The effective energy storage after a cycle of injection $E_{storage}$ can be calculated by Eq. (5).

$$E_{storage} = \sum_{i=1}^{n} \left(T_{ground,mod} - T_{ground,nat}\right) \cdot c_{ground} \cdot \rho_{ground} \cdot V_{ground} \quad (5)$$

Where $T_{ground,nat}$ is the natural ground temperature, before heat injection, $T_{ground,mod}$ is the modified ground temperature, at the end of the injection period, $c_{p\ ground}$ is the specific heat of the ground interested by the injection, ρ_{ground} is the density of the ground interested by the injection, V_{ground} is the volume of the ground interested by the heat injection. Regarding the latter, it is preliminarily considered of regular cylindrical shape, with the center in the middle of the BTES; however,

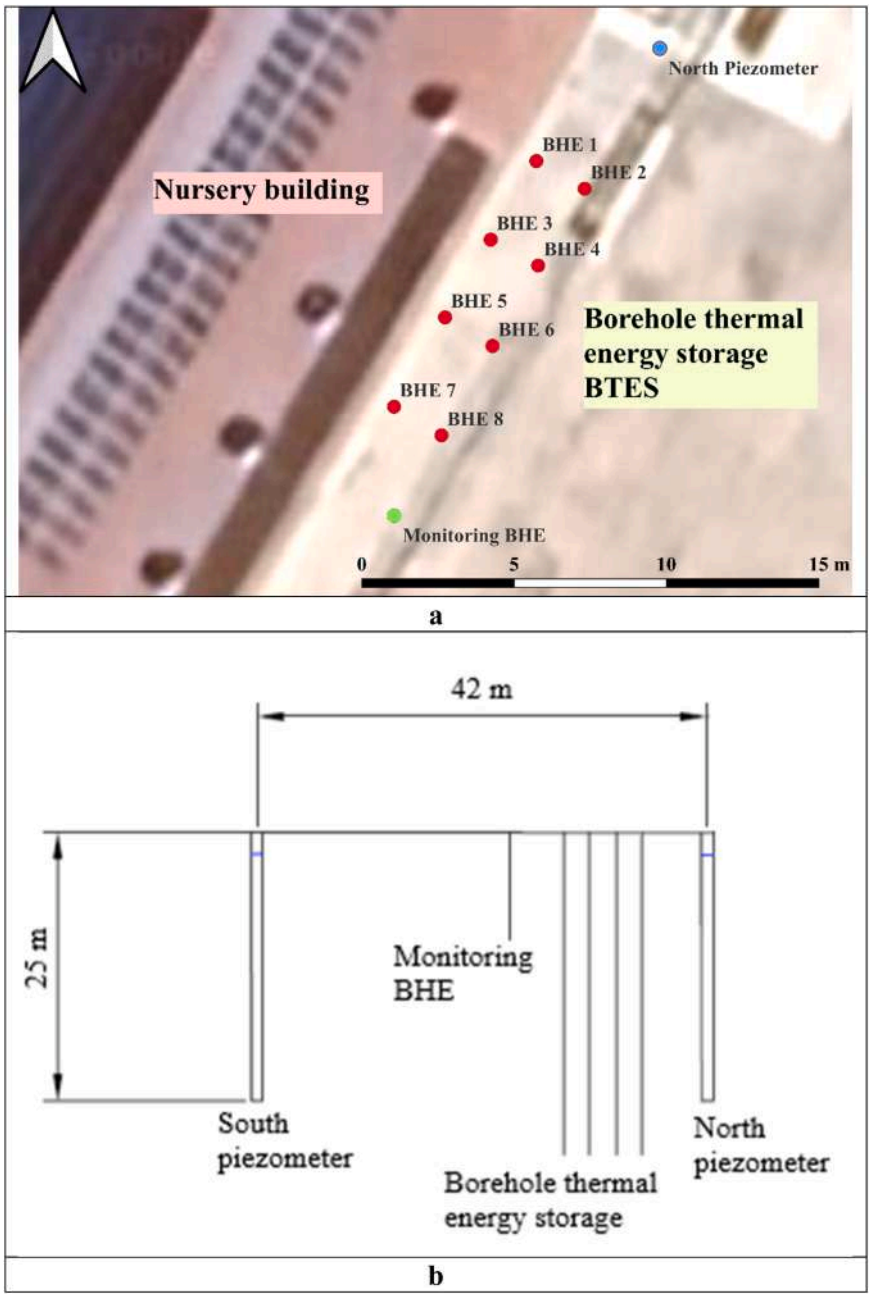

Fig. 5. Map (a) and section (b) of the BTES and the ground monitoring system.

Table 1
Energy loads used for modeling and design.

	Design ground energy exploitation (MJ)	Design solar energy injection (MJ)
Jan	16,210.8	3254.4
Feb	15,991.2	3754.8
Mar	6505.2	8964.0
Apr	2916.0	9792.0
May	1454.4	13,831.2
Jun	39.6	13,446.0
Jul	3.6	17,121.6
Aug	3.6	14,342.4
Sep	93.6	10,292.4
Oct	4136.4	6858.0
Nov	8348.4	3646.8
Dec	14,274.0	3618.0
TOT	69,973.2	108,921.6

the geometry can be potentially affected by the impact of groundwater movement.

In terms of performance of the DSHP, the theoretical coefficient of performance (COP), for both ground and air source, is presented below.

$$COP_{ideal,ground} = \frac{T_{out,building}}{T_{out,building} - T_{in,BTES}} \quad (6)$$

$$COP_{ideal,air} = \frac{T_{out,building}}{T_{out,building} - T_{in,air}} \quad (7)$$

On the other hand, the effective performance of the DSHP is evaluated by the practical COP, ratio between the heat provided and the electric power absorbed, and the related monthly and seasonal performance factors (MPF and SPF)

$$COP_{effective} = \frac{H}{P} \quad (8)$$

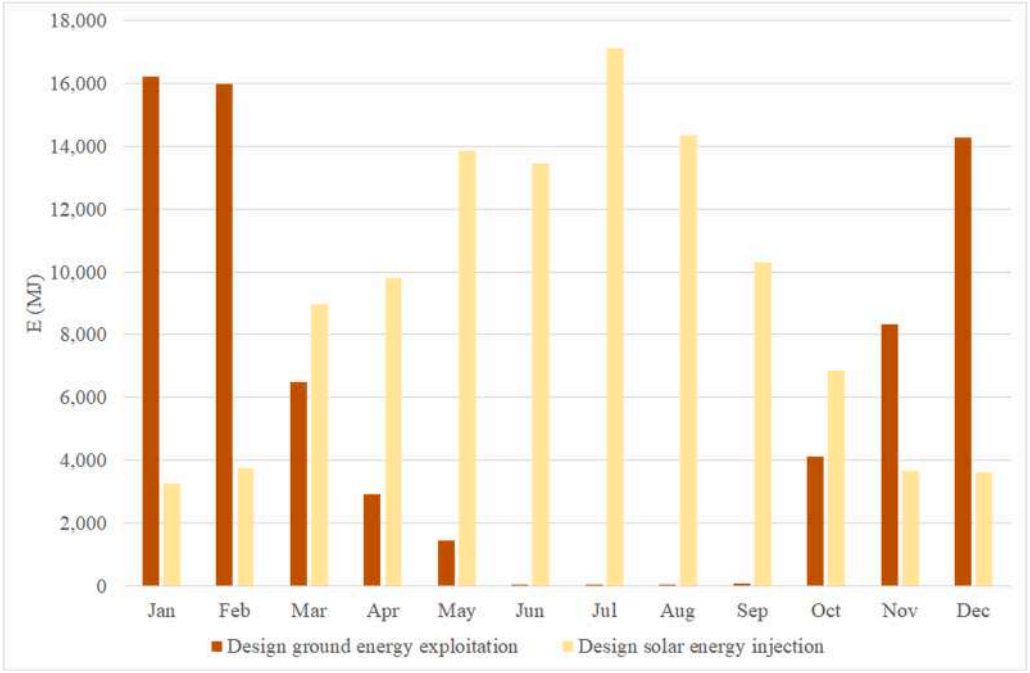

Fig. 6. Design energy loads.

Table 2
Coefficient of performance design data of the DSHP.

Heat source temperature (°C)		Heat pump COP
Water	Air	
-	1	2.5
0	6	2.8
5	11	3.0
10	16	3.4
15	21	3.9
20	26	4.5
25	31	5.0

$$\boldsymbol{MPF_i} = \frac{\boldsymbol{E_{building.i}}}{\boldsymbol{L_i}} \tag{9}$$

$$\boldsymbol{SPF} = \frac{\sum_{i=1}^{n} \boldsymbol{E_{building.i}}}{\sum_{i=1}^{n} \boldsymbol{L_i}} \tag{10}$$

Where H is the thermal power provided (W), P is the electric power absorbed (W) and L_i is the electric energy absorbed in the month i.

For the air mode, P and L_i refer to the works of compressor and fans; for the ground mode, P and L_i refer to the work of compressor and circulation pumps; finally, for the hybrid mode, P and L_i refer to the combined work of compressor, fans and circulation pumps.

Excluding the auxiliaries, the MPFs and SPF can be calculated by knowing the ambient energy. In this case, the values are always higher, and the equations are as follows:

$$\boldsymbol{MPF_i} = \frac{\boldsymbol{E_{building.i}}}{\boldsymbol{E_{building.i}} - \boldsymbol{E_{ambient.i}}} \tag{11}$$

$$\boldsymbol{SPF} = \frac{\sum_{i=1}^{n} \boldsymbol{E_{building.i}}}{\sum_{i=1}^{n} \left(\boldsymbol{E_{building.i}} - \boldsymbol{E_{ambient.i}}\right)} \tag{12}$$

3. The case study

The Golinelli swine farm is located in Mirandola, in the province of Modena (northern Italy), and rears 500 sows and 2500 weaners. The farm consists of a farrowing barn, a nursery barn, a gestation barn, and a hog barn with a gestation sector. The goal of the RES4LIVE project was to demonstrate the efficiency of renewable heating and electricity for the nursery barn. In such building, originally, heating was provided by a 34 kW LPG boiler, supported by 5 thermal lamps within each of the 10 nursery rooms (Fig. 1). The fossil-fueled boiler was then replaced by the integrated PVT-BTES-DSHP system (Fig. 2), consisting of: a 35-kW_{th} dual source heat pump (DSHP), able to select the ambient source (air or ground) as an alternative or in combination (Fig. 2a);

- a BTES field consisting of 8 double-U BHE, 30 m deep, occupying around 18 m^2 of the courtyard (Fig. 2b);
- a PVT system formed by 24 SAMSTER SunPro 320 W PVT collectors, with a total electric and thermal capacity of 25 kW_{th} and 7.68 kW_{el}, respectively, and covering 39.3 m^2 of the building roof (Fig. 2c);
- a solar central station with a novel standardized design, the heart of the system, able to switch the direction of the flows according to the needs (Fig. 2d).

The solar station consists of an uninsulated PVT field hydraulically connected to the BTES. The circulation pump between the PVT field and the BTES is governed by a rule-based control strategy designed to ensure positive heat transfer and avoid unnecessary parasitic consumption. The pump is activated when either of the following conditions is satisfied: The global irradiance on the collector plane exceeds 150 W/m^2, ensuring sufficient solar availability;

- The temperature difference between the PVT outlet temperature and the BTES return temperature exceeds 4 °C, ensuring a favorable thermal gradient for heat injection into storage.

Subsequently, the pump is deactivated when both conditions fall below these thresholds, preventing operation under low-gain or thermodynamically unfavorable conditions.

Specifically to the DSHP providing heat to the nursery building, it is activated via a remote dry contact from the farm's central management. The system's performance and critical operational parameters—such as temperatures, pressures, and equipment status—are continuously

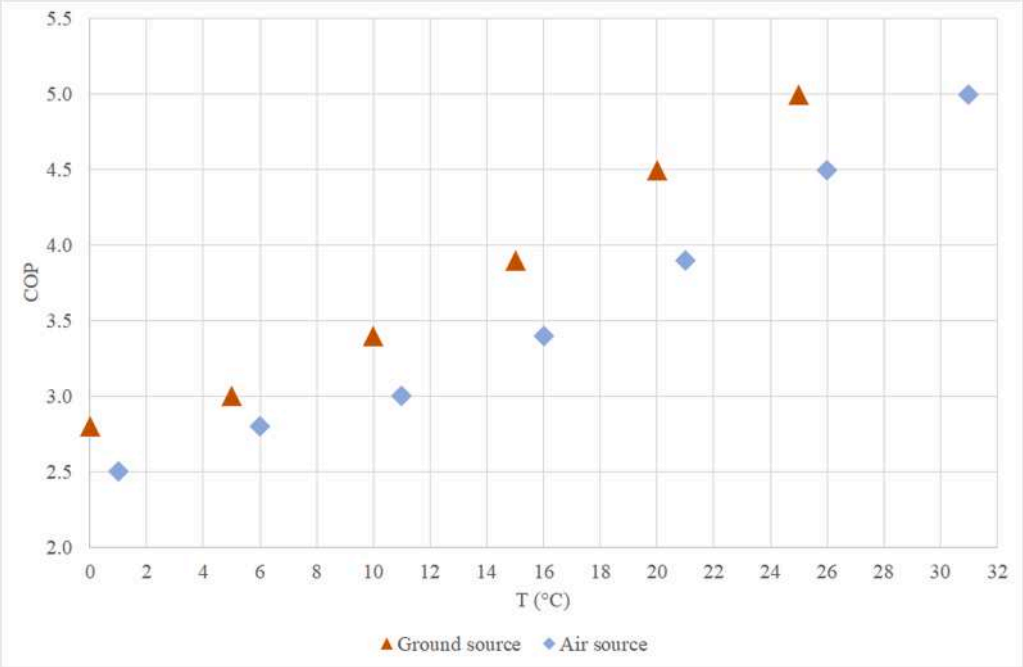

Fig. 7. COP design data of the DSHP.

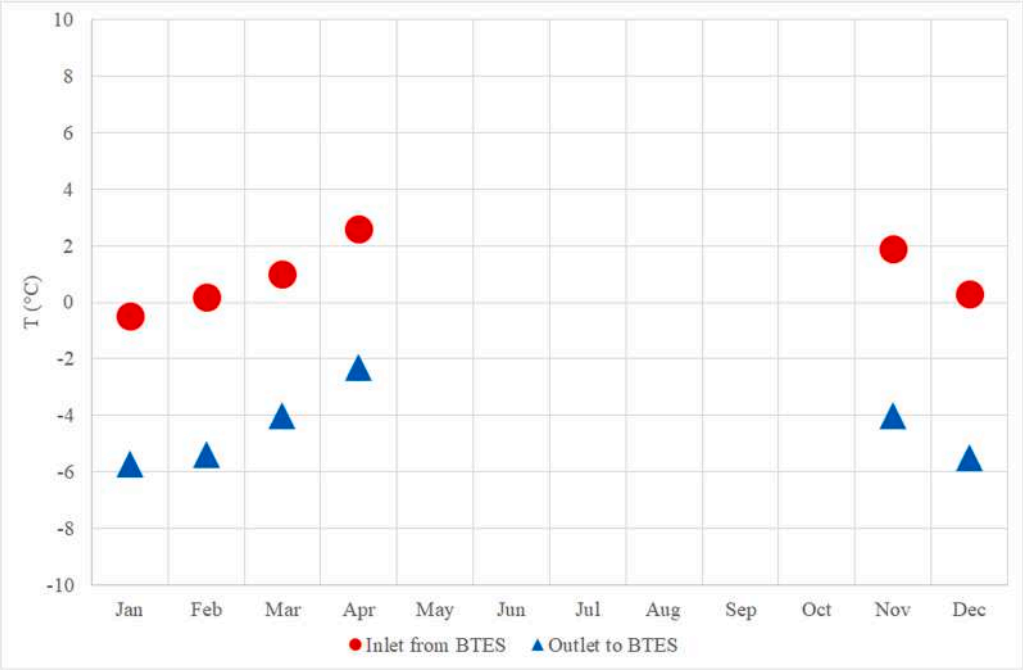

Fig. 8. Average minimum temperature in the DSHP-BTES circuit for the various months.

logged and monitored on a cloud-based platform via Modbus TCP. The core operation is governed by a Mitsubishi FX5U PLC, which provides robust control over the entire system architecture. To meet the specific thermal demands of the facility, the system is designed to maintain a constant supply water temperature setpoint of 50–55 °C. This is achieved using a Copeland digital scroll compressor, which dynamically modulates its capacity based on the required heating load. Furthermore, the refrigerant flow is precisely managed by two Electronic Expansion Valves (EEVs), each dedicated to one of the two evaporators (water-cooled and air-cooled). The FX5U PLC regulates these EEVs utilizing two independent Proportional-Integral-Derivative (PID) control loops, ensuring optimal superheat and stability across all operating modes.

To maximize the overall Coefficient of Performance (COP), the control algorithm prioritizes the highly efficient water-cooled evaporator, dynamically adjusting the heat source based on the glycol inlet temperature. The specific temperature setpoints governing these source transitions were established as optimal for the heat pump's efficiency following extensive experimental trials. When the glycol temperature is above 4 °C (plus a predefined differential), the system operates solely on the water-cooled source. A drop below 4 °C triggers a hybrid mode, activating the air-cooled evaporator simultaneously. For freeze protection, a critical safety setpoint is set at −1 °C; below this threshold, the

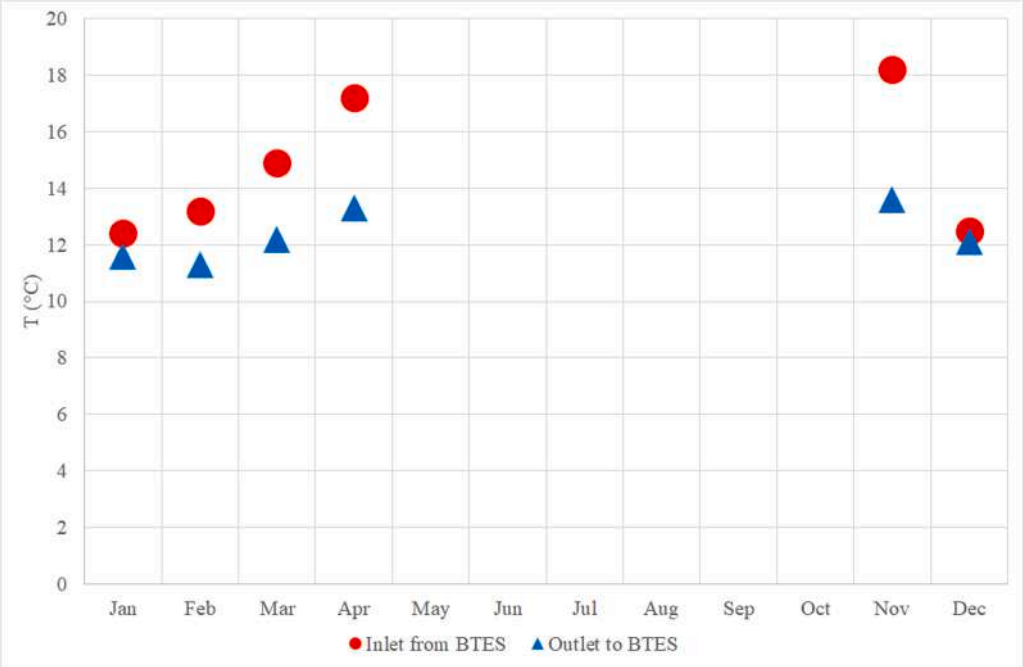

Fig. 9. Average maximum temperature in the DSHP-BTES circuit for the various months.

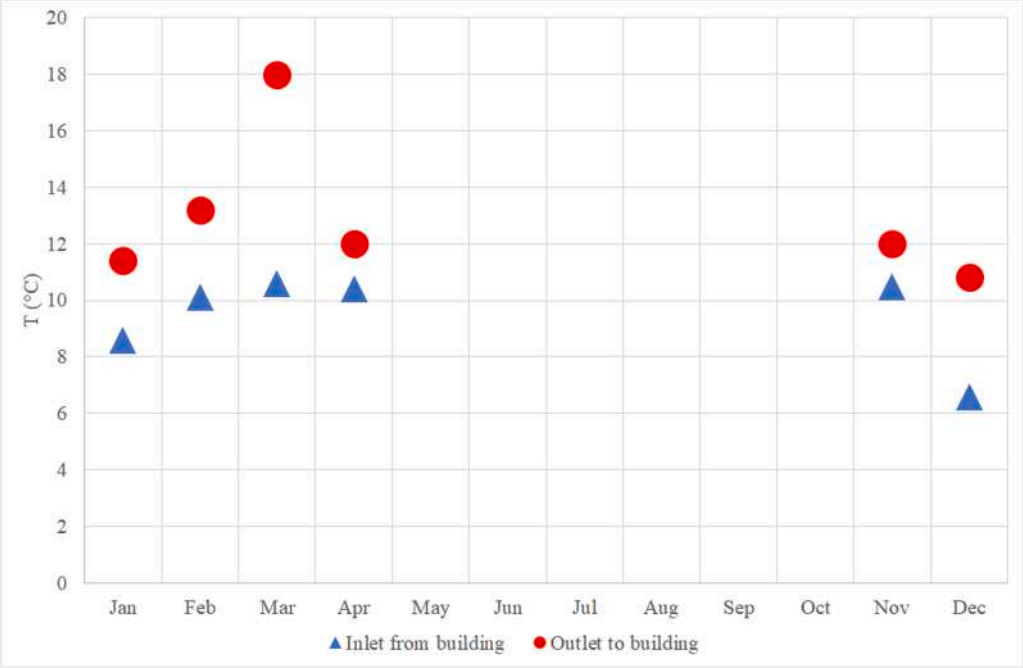

Fig. 10. Average minimum temperature in the DSHP-building circuit for the various months.

water-cooled evaporator is entirely bypassed, and heating relies exclusively on the air-cooled source. Finally, frost accumulation on the air coil is managed via a hot gas bypass valve, supported by backup electrical resistors for severe ambient conditions where hot gas alone is insufficient.

Finally, PLEGMA Labs provided a fully integrated measuring and monitoring system of both the ambient variables of the nursery barn and of the working variables of the PVT-BTES-DSHP plant. The schematic of the integrated PVT-BTES-DSHP system is presented in Fig. 3. Additionally, the detail of the schematic of the DSHP, and its connection to the building and the BTES, is illustrated in Fig. 4.

The BTES and ground temperature monitoring system is composed by eight BHE 30 m deep, one monitoring BHE 10 m deep, and two monitoring piezometers, 25 m deep and located respectively upwards and downwards of the BHE field, along the groundwater flow direction. The connection among BHEs was tailored for the heat storage optimization and subsequent recovery within the PVT-BTES-DSHP system; its exact configuration is currently patented. (Fig. 5)

The energy loads exposed in Table 1 and Fig. 6 were originally used for the modeling and design of the integrated PVT-BTES-DSHP system. The ground energy exploitation loads were found based on the building heat request in a reference year, while the solar energy injection loads

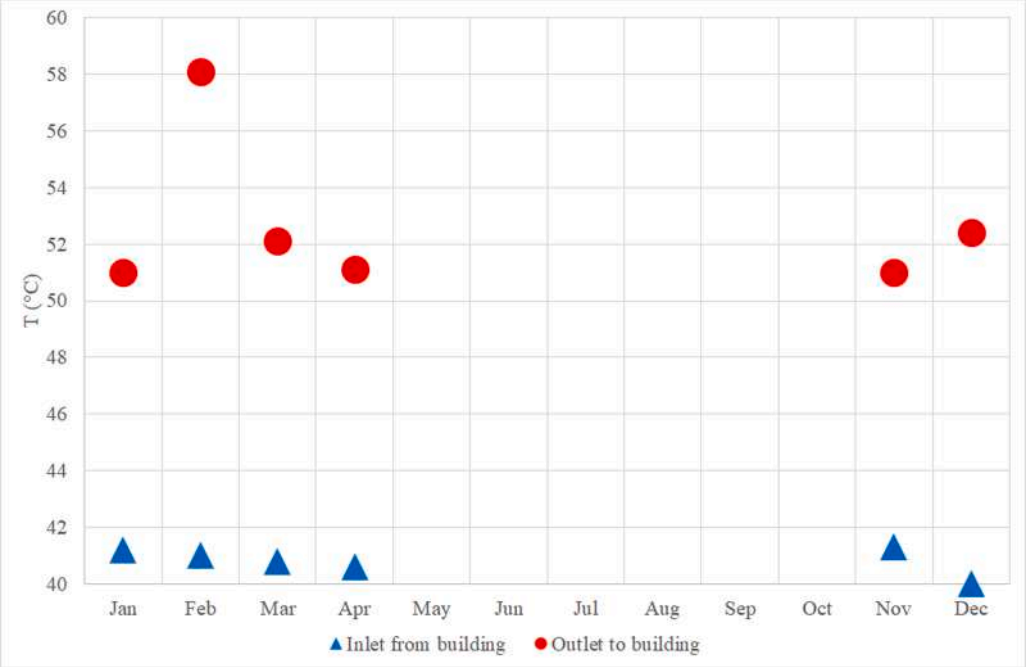

Fig. 11. Average maximum temperature in the DSHP-building circuit for the various months.

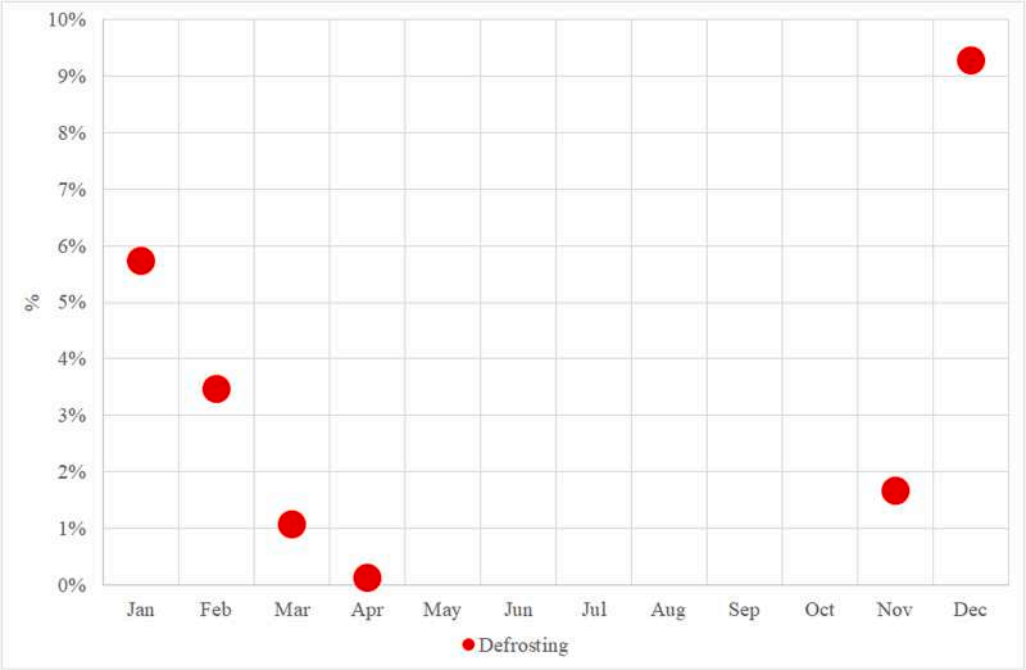

Fig. 12. Defrosting of fans occurrence for the various months.

were found by using an average value of the solar irradiation of the previous ten years and by imposing the temperature injection limit in the BTES of 35 °C, due to the local environmental regulations for aquifer protection. Moreover, such loads are not supposed to cover the whole demand of the nursery barn, since the peak power is covered by the air source.

By design, PVT electrical production is expected to be approximately 40 MJ/year. This value has not yet been verifiable experimentally as the PVT's electricity production was not yet connected to the grid due to a delay caused by local regulatory issues.

With respect to the coefficient of performance (COP) of the DSHP, it is presented in Table 2 and Fig. 7.

The activation of the fans (air source) is based on two temperature levels of the geothermal circuit (outlet from the heat pump and return to the BTES). The first level is imposed at 4 °C. When the fluid outlet temperature drops below this value, the fans activate and the air source is exploited as an integration of the ground source, to reach the peak thermal power of 35 kW. The second level is imposed at −1 °C. When the fluid outlet temperature drops below this value, the geothermal circuit is shut down and the air source covers entirely the power. In both cases, the heat release in the geothermal circuit makes the ground recovers, for a soon reactivation. Due to the use of antifreeze, working temperatures

Table 3
Comprehensive results of the DSHP for the first monitoring year.

	Thermal energy provided to the building (MJ)	Electric energy full consumption (MJ)	Monthly Performance Factor (MPF)
Jan	32,440.32	8419.54	3.85
Feb	19,614.42	5161.36	3.80
Mar	15,223.36	4119.37	3.70
Apr	4873.79	1200.58	4.06
May			-
Jun			-
Jul			-
Aug			-
Sep	38.81	7.152	5.42
Oct			-
Nov	34,685.57	8971.75	3.87
Dec	40,250.81	11,037.32	3.65
TOT	147,132.72	38,917.07	3.78

up to −10 °C can be reached by the circulating fluid.

3. Results and discussion

Within the first monitoring year, the temperature of the various fluids involved, and the working and energy data of the DSHP, were recorded every minute. For each month, the average minimum and maximum working temperature at both BTES and building side were calculated and the results are presented. Fig. 8 shows the average minimum temperatures recorded at the outlet of the BTES–DSHP circuit for each month. These values provide a direct indication of the lowest geothermal source temperatures exploited by the heat pump during operation. The results highlight that, even during the coldest winter months (December–February), the minimum fluid temperature remains safely above the lower operational threshold imposed by the control strategy. This confirms that the combination of shallow geothermal exchange and prior solar heat injection effectively prevents excessive cooling of the ground. Moreover, the relatively stable minimum temperatures observed from November to March indicate that the BTES was not thermally depleted, despite sustained heat extraction during the heating season. Fig. 9 presents the corresponding average maximum temperatures in the BTES–DSHP circuit. These values reflect periods when either solar-charged ground volumes or partial recovery phases contributed to raising the inlet temperature to the heat pump. The gradual increase in maximum temperatures observed during late winter and early spring suggests a progressive thermal recovery of the BTES, supported by reduced heating demand and occasional simultaneous solar heat injection. This behaviour confirms the dynamic and reversible nature of the storage system, which can both supply and recover heat depending on seasonal conditions. Fig. 10 reports the average minimum temperatures measured on the DSHP–building circuit, representing the lowest supply conditions delivered to the heating distribution system of the nursery barn. The data demonstrate that the system consistently maintained minimum supply temperatures compatible with the thermal requirements of the livestock building, even during mild season demand winter demand. The absence of critical temperature drops confirms the adequacy of the DSHP control logic and the effectiveness of the hybrid ground–air operation in ensuring continuity of service under unfavourable climatic conditions. Fig. 11 shows the average maximum temperatures recorded on the DSHP–building circuit. These values are associated with periods of the highest thermal demand by the barn, with

Table 4
Comprehensive results of the DSHP for the first year, excluding the auxiliaries.

	Thermal energy provided to the building (MJ)	Ambient energy (All sources) (MJ)	Monthly Performance Factor (MPF)
Jan	32,440.32	24,416.46	4.04
Feb	19,614.42	14,715.79	4.00
Mar	15,223.36	11,138.58	3.73
Apr	4873.79	3716.64	4.21
May			-
Jun			-
Jul			-
Aug			-
Sep	38.81	31.68	5.44
Oct			-
Nov	34,685.57	25,858.01	3.93
Dec	40,250.81	29,543.58	3.76
TOT	147,132.72	109,425.02	3.90

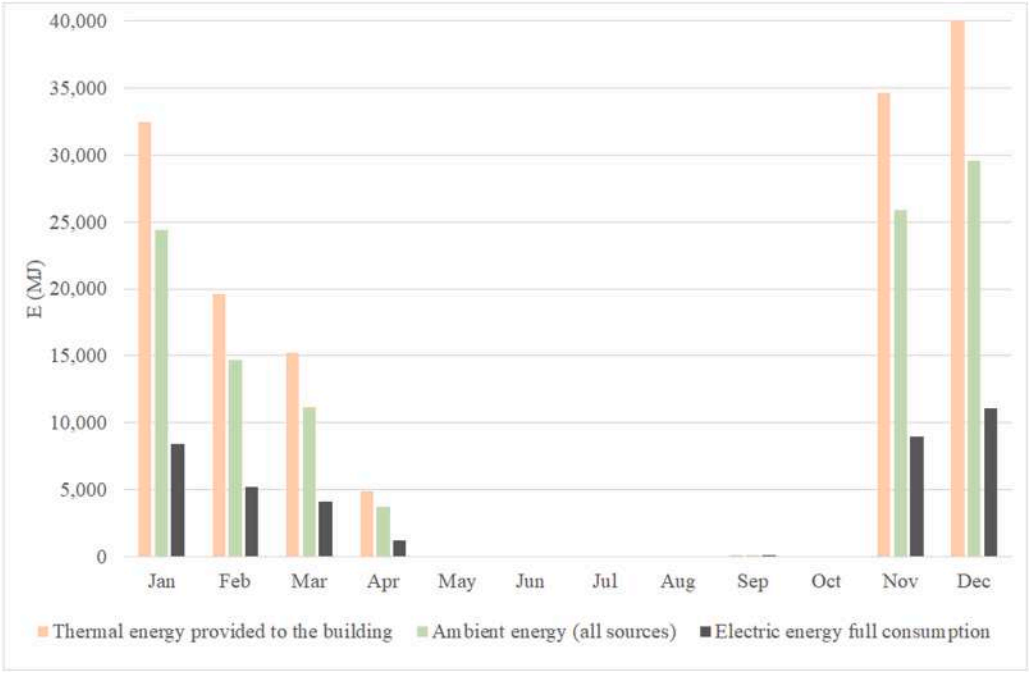

Fig. 13. Comprehensive results of the first year of use.

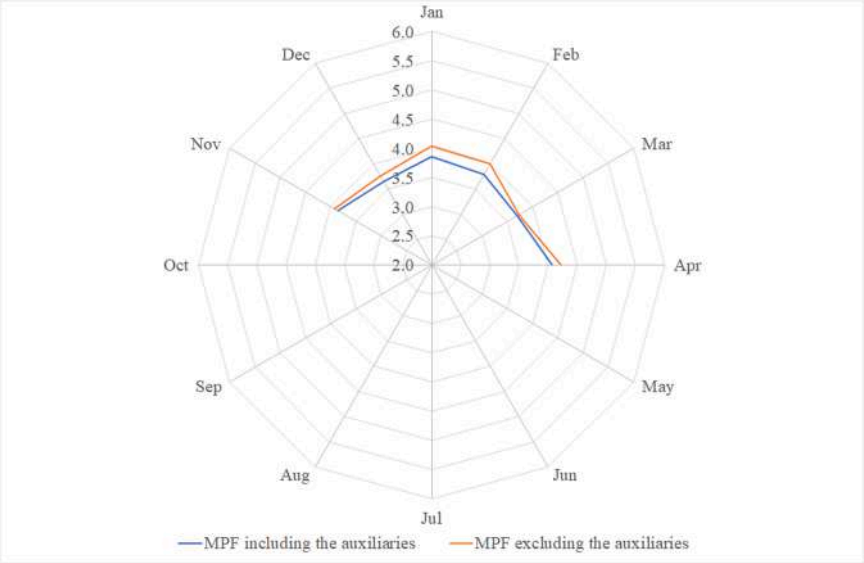

Fig. 14. Impact of the auxiliaries' electric energy consumption over the monthly performance factor.

Table 5
Detailed results of the working type of the DSHP for the first monitoring year.

	Ground only energy source (MJ)	Air only energy source (MJ)	Hybrid energy (ground+air) source (MJ)
Jan	9314.06	2478.64	12,656.70
Feb	6636.78	454.03	7645.00
Mar	2852.21	0	8286.62
Apr	2788.70	0	925.52
May	0	0	0
Jun	0	0	0
Jul	0	0	0
Aug	0	0	0
Sep	31.68	0	0
Oct	0	0	0
Nov	8602.13	823.32	16,430.29
Dec	12,003.44	2836.98	14,789.05
TOT	42,230.66	6592.97	60,735.85

contemporary enhanced source availability, during which the heat pump operates at higher condenser temperatures. The relatively narrow range of maximum temperatures across the heating season reflects stable system regulation and avoids excessive temperature fluctuations inside the building, which is particularly important for maintaining animal welfare and preventing thermal stress.

Details of defrosting is presented in Fig. 12. The system worked from November to April, while it was completely shut down in the other months; defrosting occurred 3.6 % of the time in the mentioned period. Table 3 summarises the comprehensive energetic performance of the DSHP during the first year of operation, including the electric energy consumption of the compressor and all auxiliaries (circulation pumps and fans). The reported results refer exclusively to periods of active system operation and provide a complete overview of monthly heat delivery, electricity use, and resulting MPFs. The system supplied a total of 147,133 MJ of thermal energy to the nursery building over the monitoring year, with an associated electric energy consumption of 38,917 MJ, resulting in an overall Seasonal Performance Factor (SPF) of 3.78. These values confirm the high efficiency of the integrated PVT–BTES–DSHP system, particularly considering the shallow depth of the borehole field and the intermittent nature of the heating demand in livestock buildings. The monthly distribution of heat production clearly reflects the seasonal heating requirements of the nursery barn. The highest thermal outputs were recorded in December (40,251 MJ) and November (34,686 MJ), followed by January (32,440 MJ), corresponding to the coldest months of the year. In contrast, heat demand progressively decreased during spring, with limited operation in March (15,223 MJ) and April (4874 MJ), and negligible operation outside the heating season. The small amount of heat delivered in September is attributable to a short functional test of the DSHP and does not represent regular operation. Electricity consumption followed a similar seasonal trend, peaking in winter months when both the compressor load and auxiliary operation increased due to lower source temperatures and higher heating demand. Despite this, the MPF values remained relatively stable throughout the heating season, ranging between 3.65 and 4.06, with the highest MPF observed in April (4.06). This indicates that system efficiency was not significantly degraded during periods of high demand, highlighting the effectiveness of the dual-source operating strategy and the contribution of solar-assisted geothermal storage. Fig. 13 graphically illustrates the relationship between thermal energy supplied to the building and the corresponding electrical energy consumption for each month. The figure clearly shows that increases in delivered heat are not associated with proportional increases in electricity use, confirming the favourable thermodynamic behaviour of the system. The consistent gap between the heat output and the electric input across the heating season visually reinforces the robustness of the achieved MPFs.

Table 4 present the energetic performance of the dual-source heat pump (DSHP) during the first monitoring year excluding the electrical consumption of auxiliary components, such as circulation pumps and fans. In this analysis, the Monthly Performance Factors (MPFs) are calculated considering only the ambient energy extracted from the heat sources (ground, air, or their combination), thus providing an upper-bound estimate of the thermodynamic performance of the heat pump itself. In order to deliver the thermal energy needed to the building, as depicted in Table 4, the system extracted 109,425 MJ of ambient energy from renewable sources, resulting in an overall SPF of 3.90 when auxiliaries are excluded. Compared with the comprehensive SPF of 3.78 reported in Table 3, this corresponds to a relative difference of approximately 3 %, highlighting that auxiliary electricity consumption has a limited impact on the overall efficiency of the system. The monthly values show a consistent trend across the heating season. During winter months (November–February), MPFs range between 3.76 and 4.04, demonstrating that high efficiency is maintained even under unfavourable climatic conditions. Slightly higher MPFs are observed during transitional periods, such as April (4.21) and September (5.44), when

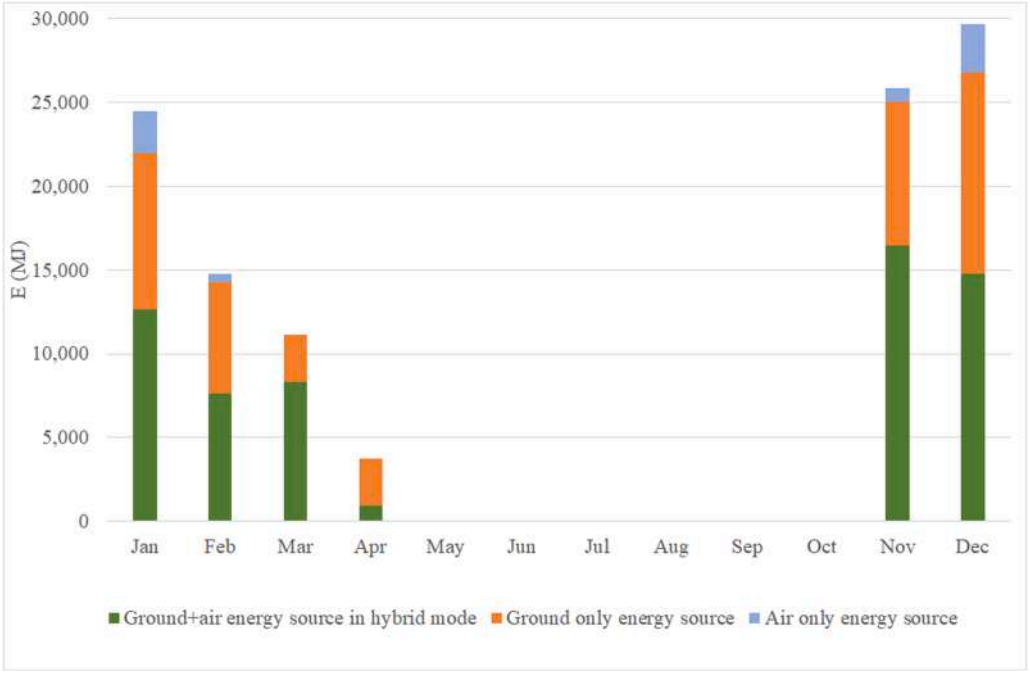

Fig. 15. Detailed results of the working mode.

Table 6
Detailed results of the use of ground source by DSHP for the first monitoring year.

	Ground energy source (total) (MJ)	Ground only energy source (MJ)	Ground energy source in hybrid mode (MJ)
Jan	11,416.46	9314.06	2102.40
Feb	7820.75	6636.78	1183.93
Mar	3811.79	2852.21	959.58
Apr	2969.28	2788.70	180.58
May	0	0	0
Jun	0	0	0
Jul	0	0	0
Aug	0	0	0
Sep	31.68	31.68	0
Oct	0	0	0
Nov	11,539.51	8602.13	2937.38
Dec	14,424.66	12,003.44	2421.22
TOT	53,905.10	42,230.66	11,674.44

milder outdoor temperatures and reduced heating demand allow the DSHP to operate under more favourable source and load conditions. The September values, however, are associated with short testing periods and should not be interpreted as representative of seasonal operation.

Fig. 14 provides a visual comparison between MPFs calculated with and without auxiliary electricity consumption, clearly illustrating the marginal influence of auxiliaries on system performance. The relatively small gap between the two curves confirms that the electrical demand of pumps and fans is well balanced with respect to the heat delivered and does not significantly penalise the efficiency gains achieved through solar-assisted geothermal storage and dual-source operation. The results also indicate that the system design successfully minimised parasitic losses by limiting borehole depth, optimising hydraulic layouts, and adopting a control strategy that activates the air source only when strictly necessary. This is particularly relevant for shallow geothermal systems, where excessive auxiliary consumption can otherwise offset the benefits of ground-source operation. These results demonstrates that the core thermodynamic performance of the DSHP is high and that the inclusion of auxiliary components results in only a modest efficiency reduction.

The monitoring system recorded all working parameters of the DSHP, including selection of the operating modes and related heat provision to the building. Therefore, it was possible to clearly distinguishing the energy source at each time interval, especially in the configurations ground-source only and air-source only. Related to the hybrid ground-air operation, some additional calculations were needed and specifically Eq. (2) was used to calculate the heat exploitation from the ground based on inlet and outlet fluid temperature. In such configuration, the heat exploitation from air was obtained by subtracting the energy measured from the system and the result of the calculation, for each time interval.

Table 5 and Fig. 15 describe the distribution of thermal energy extracted by the DSHP according to the three possible operating modes: ground-source only, air-source only, and hybrid ground–air operation. With respect to the whole amount of ambient energy exploited in the monitoring year, 38.6 % was supplied exclusively by the ground source, 6.0 % by the air source alone, and the remaining 55.4 % through hybrid operation. The monthly distribution highlights a clear seasonal pattern. During the coldest months (December–February), hybrid operation dominates, accounting for more than half of the extracted energy, as the air source is activated to support the ground source during peak heating demand. In contrast, during milder periods such as March and April, ground-only operation becomes predominant, reflecting more favourable geothermal conditions and reduced load. The air-only mode is confined to short peak-demand periods, confirming that the air source effectively functions as a backup resource rather than as the primary heat source. Table 6 and Fig. 16 focus specifically on the exploitation of the geothermal source, distinguishing between energy extracted during ground-only operation and the geothermal contribution during hybrid operation. Over the monitoring year, the DSHP extracted a total of 53,905 MJ from the ground, corresponding to approximately 49 % of the total ambient energy used. Ground-only operation accounted for 42,231 MJ, while an additional 11,674 MJ were extracted from the ground during hybrid operation. The highest geothermal extraction occurred in winter months, particularly December (14,425 MJ), November (11,540 MJ) and January (11,417 MJ), when heating demand was the highest. Despite this sustained extraction, no evidence of thermal depletion of the BTES was observed, as confirmed by stable minimum source temperatures and subsequent thermal recovery. The geothermal source

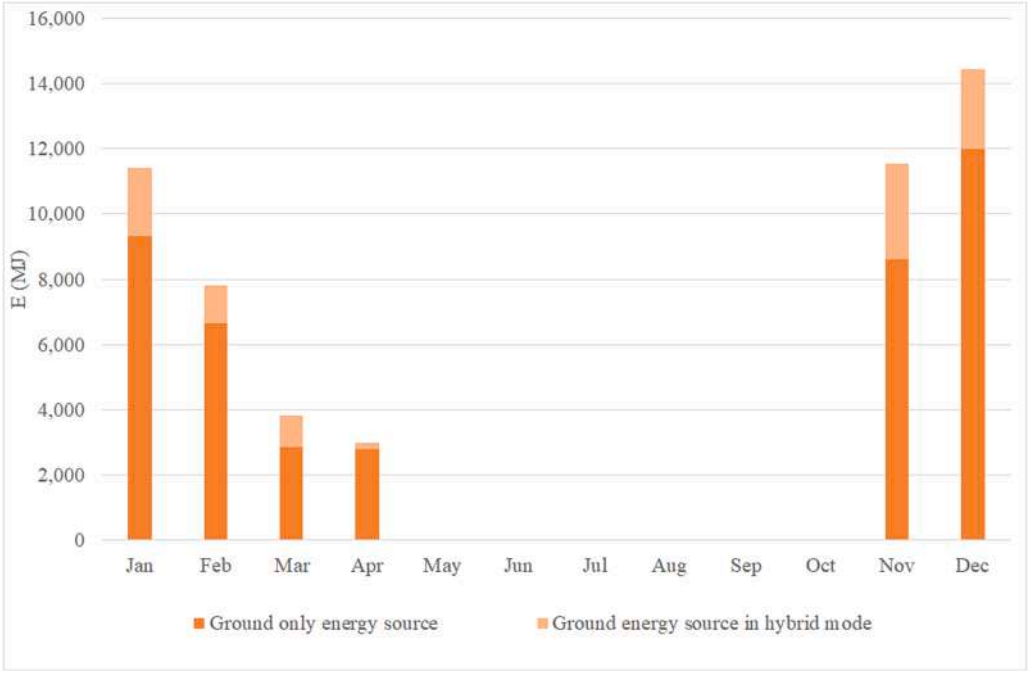

Fig. 16. Specific results of the ground source use.

Table 7
Detailed results of the use of air source by DSHP for the first monitoring year.

	Air energy source (total) (MJ)	Air only energy source (MJ)	Air energy source in hybrid mode (MJ)
Jan	13,032.90	2478.64	10,554.26
Feb	6915.06	454.03	6461.03
Mar	7327.04	0.00	7327.04
Apr	744.95	0.00	744.95
May	0.00	0.00	0.00
Jun	0.00	0.00	0.00
Jul	0.00	0.00	0.00
Aug	0.00	0.00	0.00
Sep	0.00	0.00	0.00
Oct	0.00	0.00	0.00
Nov	14,316.26	823.32	13,492.91
Dec	15,204.82	2836.98	12,367.84
TOT	55,654.38	6592.97	49,061.41

remained the dominant contributor throughout the heating season, even when the air source was activated. This confirms that the role of the air source is complementary rather than substitutive, allowing the geothermal field to operate within safe thermal limits while maintaining high system efficiency. Table 7 and Fig. 17 present the detailed contribution of the air source, distinguishing between air-only and hybrid operation. The total ambient energy extracted from the air source during the monitoring year amounted to 55,654 MJ, slightly exceeding the geothermal contribution. However, only 6593 MJ were extracted in air-only mode, while the remaining 49,061 MJ were supplied during hybrid operation. This distribution highlights that the air source is primarily exploited in conjunction with the ground source rather than independently. The air contribution peaks in winter months, particularly in December (15,205 MJ), November (14,316 MJ) and January (13,034 MJ), when outdoor temperatures are low and heating demand is high. During transitional months, air-source exploitation decreases significantly, and no air contribution is recorded outside the heating season. The air-only operation is limited to brief periods, supporting the conclusion that the air source is mainly used to cover thermal peaks and prevent excessive cooling of the ground. This strategy enhances system resilience without compromising the overall efficiency.

Finally, Table 8 and Fig. 18 shows the average COP for the various operation modes as a whole.

In terms of fluid evolution, the following Figs. 19 and 20 present the daily and monthly analysis, by selecting 15th November as typical working day and November as typical working month. In the specific condition of November, the ground is the main energy source, supplied by air, when necessary, only in hybrid mode. The daily coefficient of performance of the DSHP for 15th November was 3.66, which is similar to the average for the month of November and the entire work of the system.

The presented results were achieved by boosting the natural ground geothermal potential with the solar heat injected in the BTES. Specifically: in spring, the DSHP was on and off, so, for some days, contemporary geothermal energy extraction and solar heat injection occurred; in summer the DSHP system was off, and the BTES system was able to fully inject the solar heat from PVT; in autumn and winter, the DSHP recovered the stored heat of the previous two seasons to boost the performance of the system. The total injected heat for the reference year is presented in Table 9 and Fig. 21, which compares it with the exploited heat in the subsequent heating season.

In conclusion, for the first year of monitoring, the DSHP system worked 14.86 % of the time, corresponding to around 53 full days, almost distributed from November to beginning of April. The total SPF was about 3.78. The compressor of the DSHP worked 37.91 % of the time exploiting the ground source only, 53.93 % exploiting the combined ground and air source and 7.13 % exploiting the air source only, covering the peaks. Finally, the compressor worked 1.03 % of the time to perform defrosting of the fans during some cold winter nights.

The electric energy consumption of the DSHP was around 37,800 MJ for the reference year, calculated based on the SPF (Table 10).

The estimated electricity production from the PVT system (still not connected to the grid at the moment of the present paper) is between 36,000 and 39,600 MJ, thus covering between 95 % - 105 % of the system energy consumption, although in asynchrony operation.

After the first operation year, it was then possible to compare the design energy values with the effective results, considering the unpredictability of weather conditions. Regarding the real extracted ground energy (around 54,000 MJ), it was 23 % smaller than the design value

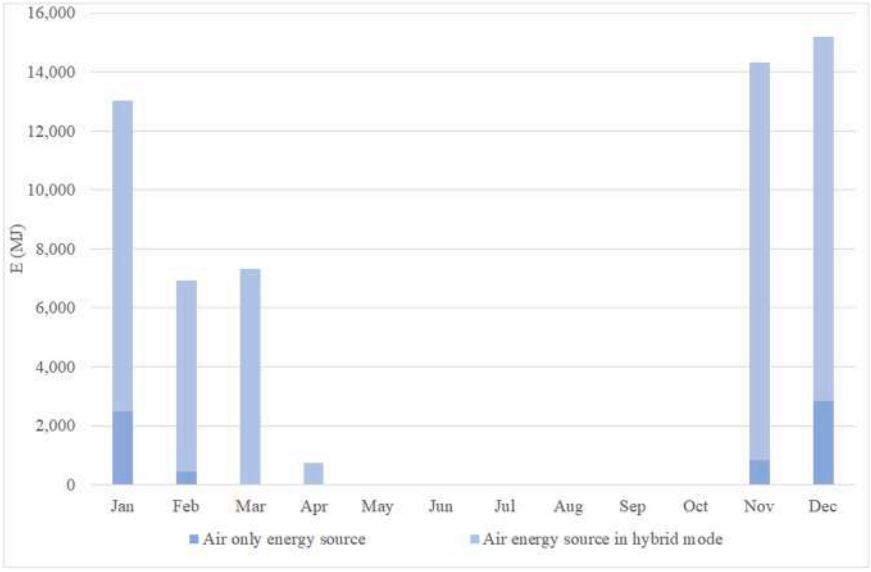

Fig. 17. Specific results of the air source use.

Table 8
Average coefficient of performance of the DSHP during the year and for the different operation modes.

	COP total	COP ground	COP air	COP hybrid
Jan	4.24	4.64	3.79	4.13
Feb	4.23	4.62	3.82	4.00
Mar	3.81	4.20	-	3.67
Apr	4.40	4.72	-	3.51
May	-	-	-	-
Jun	-	-	-	-
Jul	-	-	-	-
Aug	-	-	-	-
Sep	5.55	5.55	-	-
Oct	-	-	-	-
Nov	4.03	4.60	3.39	3.78
Dec	3.96	4.31	3.65	3.88
TOT	4.07	4.51	3.69	3.88

(around 70,200 MJ). On the other hand, the real injected solar energy (around 68,400 MJ) was 36 % smaller than the design value (around 108,000 MJ). Nonetheless, the DSHP was able, thanks to the use of air source, to provide all required energy to the building, keeping acceptable SPF (3.78).

In terms of seasonal energy storage in the subsoil, it could be calculated, by considering: the BHE temperature at the start of the extraction period, which was 20 °C, with respect to the initial ground temperature (15 °C), the volume delimited by the surface area of the BTES and their depth (30 m), thus 540 m^3 and the estimated ground volumetric heat capacity ρc_{ground} of 1.7 MJ/(m^3·K). By applying Eq. (5), the seasonal heat storage at the end of the injection period was 4590 MJ, ready for exploitation by the BHEs to fuel the DSHP.

Finally, it was possible to evaluate the impact of energy extraction and injection cycles on the aquifer, thanks to the use of two piezometers and one monitoring borehole heat exchangers, placed exactly on the direction of the groundwater movement. More details of the technical details, plan and location of the three monitoring points can be found in (Tinti, et al., 2023). Temperature strings, measuring and recording at

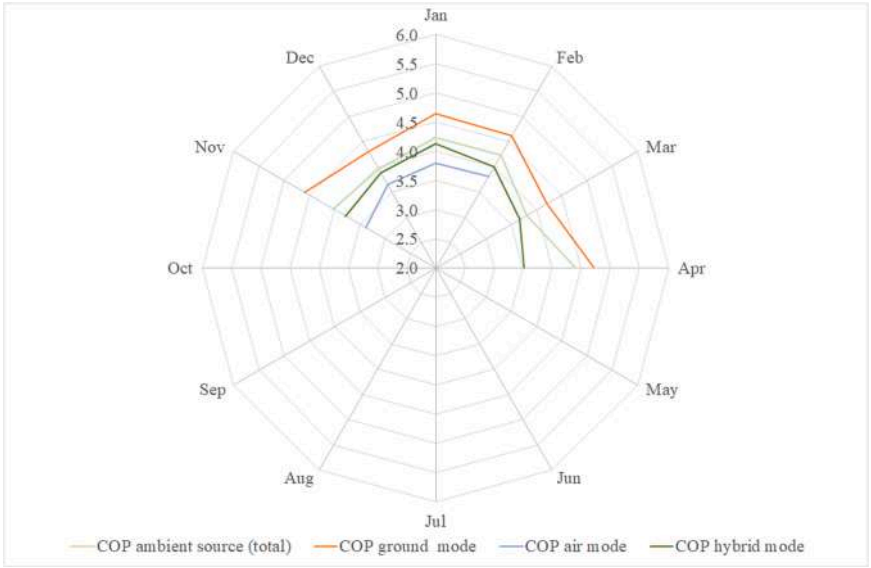

Fig. 18. Impact of the various working modes on average COP with respect to the total ambient energy data.

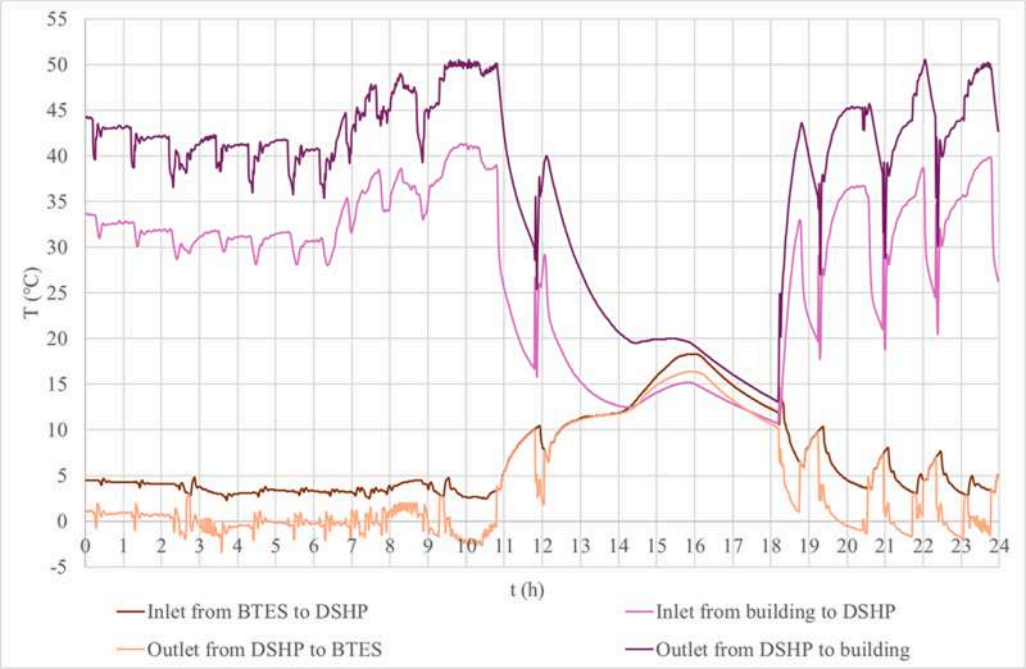

Fig. 19. Fluid temperature evolution in a typical working day (15th November).

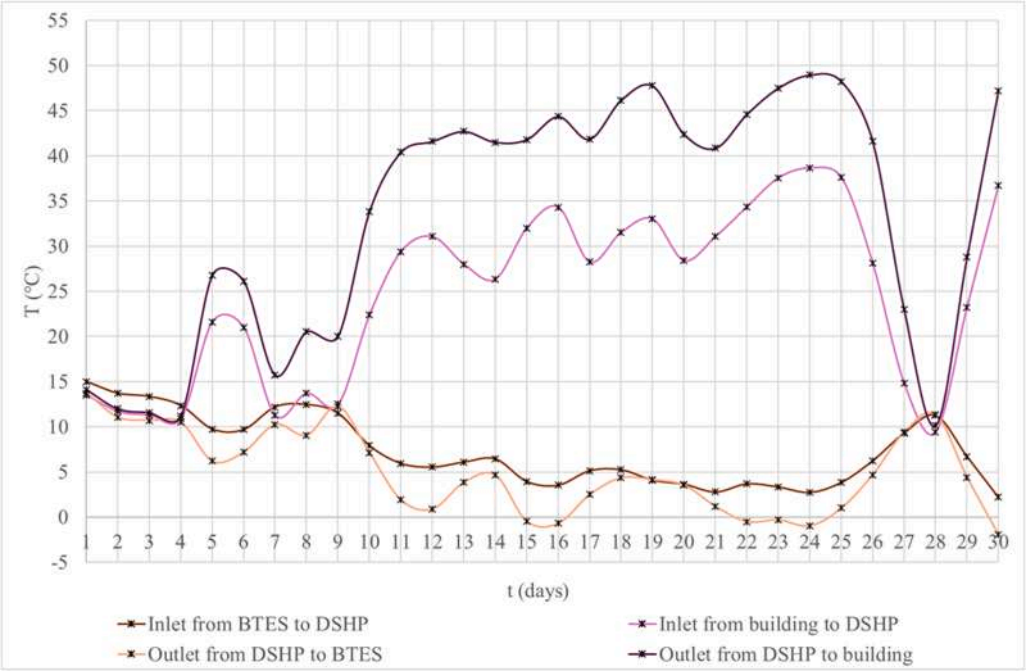

Fig. 20. Fluid temperature evolution (average values) for a typical working month (November).

each m along depth, were placed in all the three monitoring points: For the South Piezometer, upwards the BTES field and 25 m deep: from 1 to 25 m;

- For the North Piezometer, downwards the BTES field and 25 m deep: from 1 to 22 m;
- For the Monitoring BHE, upwards the BTES field (3 m far from it) and 10 m deep: from 1 to 10 m

The measured graphs are reported in Fig. 22 (South Piezometer), Fig. 23 (North Piezometer) and Fig. 24 (Monitoring BHE).

The analysis of temperatures in depth for the two piezometers are reported in Fig. 25 and Fig. 26.

By analysing the evolution of minimum, average and maximum temperature along depth, it is possible to reconstruct the model of the temperature wave and obtain useful information about the effective heat stored in the aquifer around the BTES.

The comparison of average values per month are provided by analysing the temperature difference and the amplitude at each depth. The results are presented in Figs. 27 and 28.

Finally, the average, minimum and maximum values along the monitoring BHE are instead reported in Fig. 29.

Table 9
Solar injected heat in the BTES in the first year of monitoring.

	Solar injected heat in the BTES (MJ)
Jan	1440
Feb	1800
Mar	5040
Apr	6480
May	9720
Jun	7200
Jul	13,320
Aug	12,240
Sep	5760
Oct	3240
Nov	1080
Dec	1080
TOT	68,400

The results showed how the temperature in North Piezometer is approximately 0.25 K higher than the one in South Piezometer. This can be due by the thermal impact of the solar injection in the BTES, which can be partially transferred towards North, by the groundwater movement.

In any case, the impact on the aquifer is modest and even lower than what initially simulated during the design phase (Tinti, et al., 2023). By consider the temperature difference between South and North Piezometer (around 0.22 K) entirely due by the solar heat injection, higher than the BTES heat extraction, the volume impacted by such annual storage V_{ground} can be geometrically defined by the border of the BTES towards South and by the Piezometer North, towards North (coherent with what originally modelled in (Tinti, et al., 2023)). In depth, the volume is delimited by the length of the 6 BHEs (30 m). The total calculated volume is then 900 m^3. Applying again Eq. (5), it was possible to calculate the effective annual energy storage $E_{storage}$, evidencing the impact on the aquifer, due the thermal imbalance between injected and extracted energy. The annual heat stored in the aquifer was around 340 MJ.

Such annual storage is expected to provide positive contributions along the years for the work of the DSHP, without significant impacts on the aquifer temperature (approximately a gain of 0.22 K/year in the considered area). As long-term behaviour, such imbalance will produce a thermal plume, along the groundwater flow, from South to North. By using the monitoring system installed inside the two piezometers, and especially focusing on the temperature values recorded inside the North Piezometer, it is expected to detect the thermal plume in the next three-four years. The effective influence of such thermal plume on the system's performance will be accurately analysed and object of future research.

The achieved results proved the validity of combining PVT with BTES and DSHP, where aquifer and subsoil conditions allow the underground thermal storage. With such integrated system, it was possible to reach a valuable SPF with a limited number of very shallow borehole heat exchangers: 8 BHE, 30 m deep, for a total BHE length of 240 m. As a rough comparison, in standard geothermal projects, not benefitting neither the geothermal storage and the dual source, in order to fulfil a peak power of 35 kW with such SPF, around 640 m of BHEs are necessary, almost three times the installed BHE length at the farm under study.

4. Conclusion

This study presented and analysed the first year of operation of an innovative integrated renewable energy system combining photovoltaic–thermal (PVT) collectors, borehole thermal energy storage (BTES), and a dual-source heat pump (DSHP) installed in a commercial swine nursery farm in Northern Italy. The results provide robust experimental evidence of the technical feasibility and energetic effectiveness of coupling shallow geothermal energy storage with solar-assisted heat pump systems in livestock farming applications. The specific achieved results were: Seasonal Performance Factor: 3.78. Over the monitored period, the system successfully met the thermal requirements of the nursery building, ensuring suitable indoor environmental

Table 10
Resume of electric energy consumption coherent with the SPF value.

	Heat provided to the building (MJ)	Ambient energy extraction (All sources) (MJ)	Electric energy consumption (MJ)
TOT	147,132.72	109,425.02	37,706.70

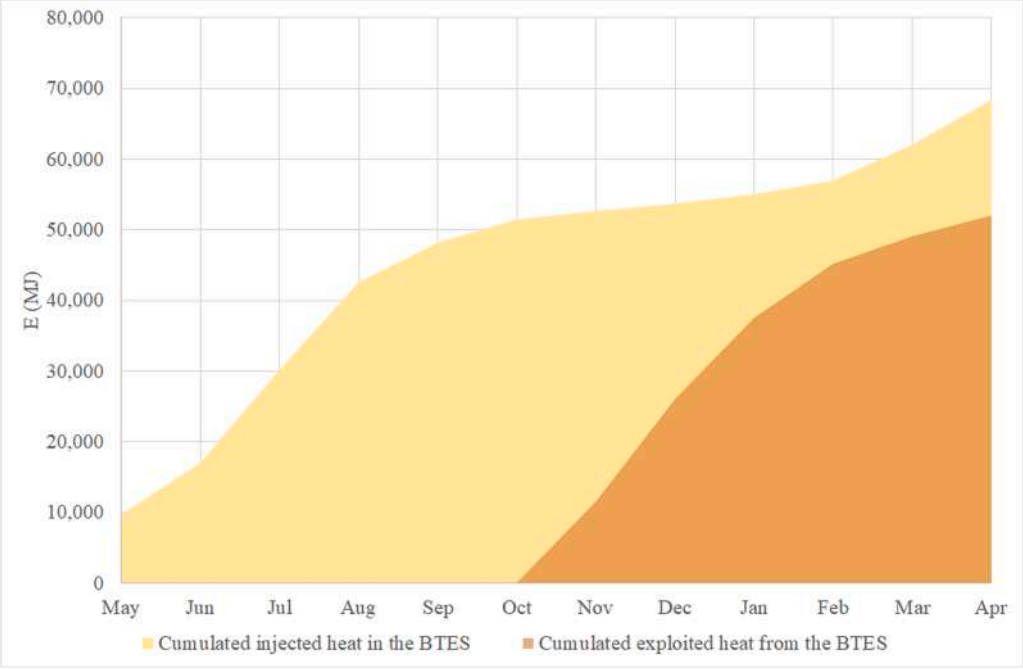

Fig. 21. Comparison of the cumulated injected and exploited energy values in the BTES for the reference year.

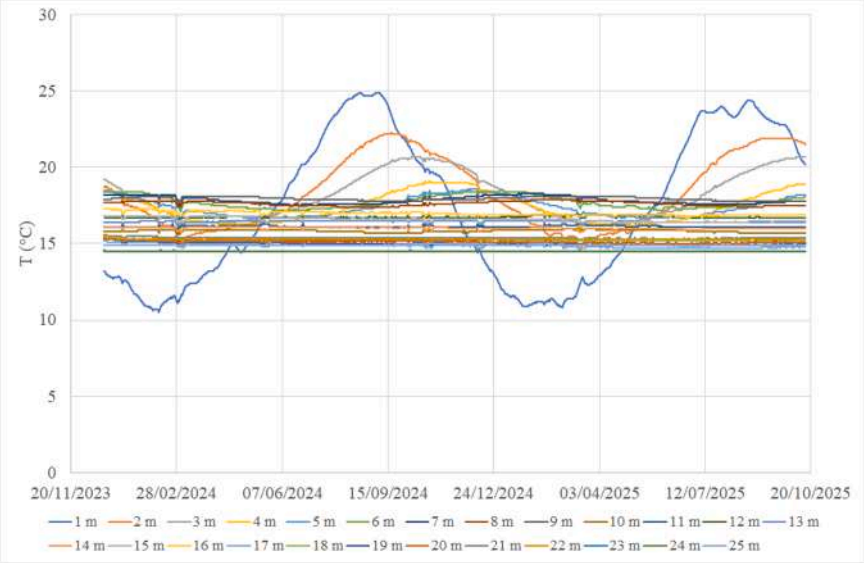

Fig. 22. Monitored subsoil temperature wave in the South Piezometer.

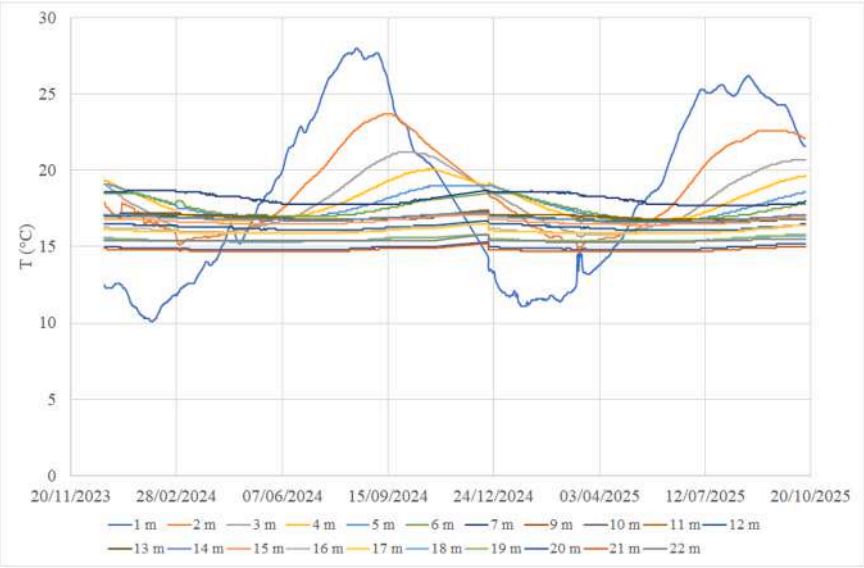

Fig. 23. Monitored subsoil temperature wave in the North Piezometer.

conditions for animal welfare while substantially reducing reliance on fossil fuels. The overall Seasonal Performance Factor (SPF) of 3.78 confirms the high efficiency of the integrated PVT–BTES–DSHP configuration, particularly considering the limited borehole depth and the stringent environmental constraints on aquifer temperature.

- Hybrid operation of the DSHP: 50 %. The hybrid operating strategy of the DSHP proved to be a key factor: approximately half of the operating time was characterised by combined ground–air operation, while exclusive air-source operation was confined to short peak-demand periods. This approach effectively prevented thermal depletion of the ground while guaranteeing continuity of service under variable climatic conditions.
- Borehole length reduction with respect to a standard GSHP project: 66 %. The seasonal solar heat injection into the BTES significantly enhanced the geothermal potential of the site. Despite deviations between design assumptions and actual weather conditions—resulting in lower-than-expected injected and extracted energy—the system maintained stable performance thanks to the flexibility of the dual-source heat pump. The measured data confirmed that solar-assisted seasonal storage can raise the effective ground temperature by several degrees, improving heat pump performance during the heating season and reducing the required total borehole length. Compared with conventional ground-source heat pump systems, the proposed solution achieved comparable thermal performance with a borehole length reduction of approximately two-thirds, highlighting its economic and spatial advantages for rural and agricultural contexts.
- Temperature variation of the shallow aquifer: 0.22 K. The dedicated monitoring network, including piezometers and a monitoring borehole aligned with groundwater flow, allowed a detailed assessment of the thermal impact on the aquifer. The observed temperature variations were modest and remained well below regulatory thresholds, confirming that the proposed system can operate safely under realistic hydrogeological conditions. The estimated annual thermal imbalance stored in the subsurface was limited, suggesting

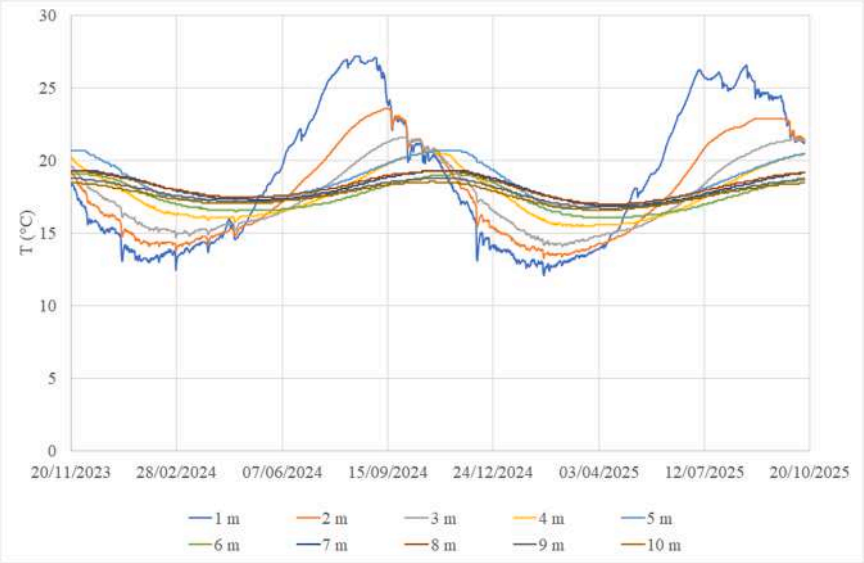

Fig. 24. Monitored subsoil temperature wave in the Borehole Heat Exchanger 3 m South of the BTES field.

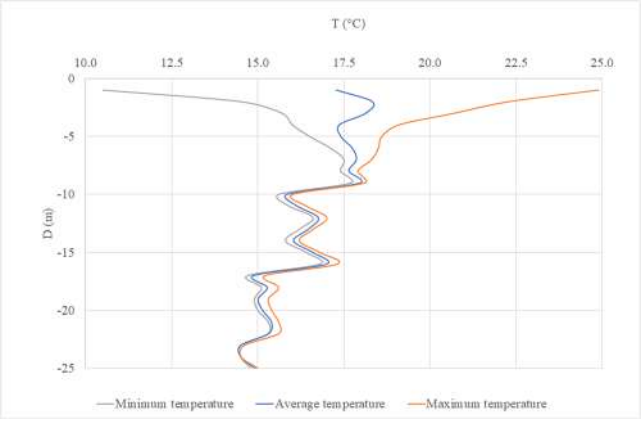

Fig. 25. Evolution of minimum, average and maximum temperature along depth for the South Piezometer.

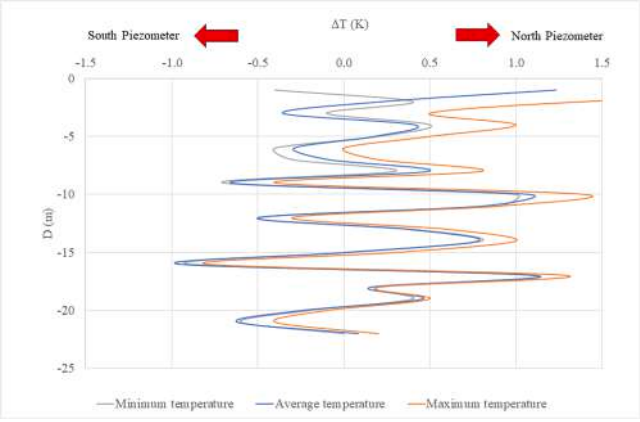

Fig. 27. Temperature difference for minimum, average and maximum values along depth between South and North Piezometer.

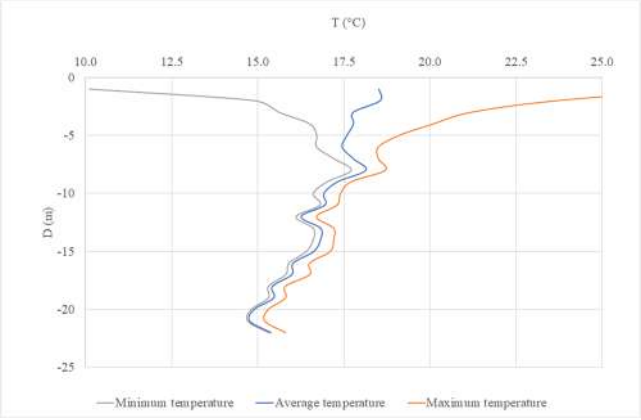

Fig. 26. Evolution of minimum, average and maximum temperature along depth for the North Piezometer.

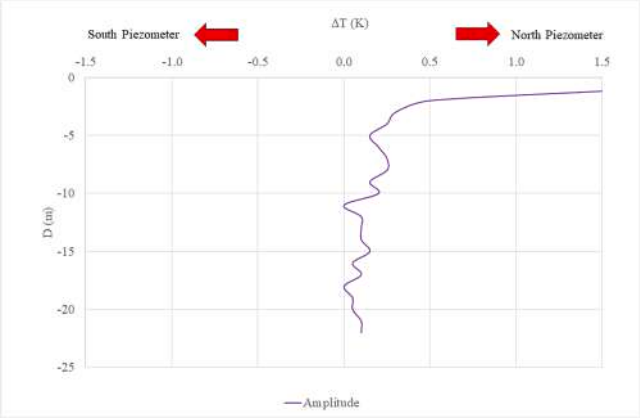

Fig. 28. Amplitude difference along depth between South and North Piezometer.

that long-term operation is unlikely to cause significant environmental impacts, while potentially providing cumulative benefits for system efficiency over successive years.

Overall, the findings demonstrate that the integration of PVT systems, BTES, and DSHP represents a promising and scalable solution for decarbonising energy use in livestock buildings. The proposed

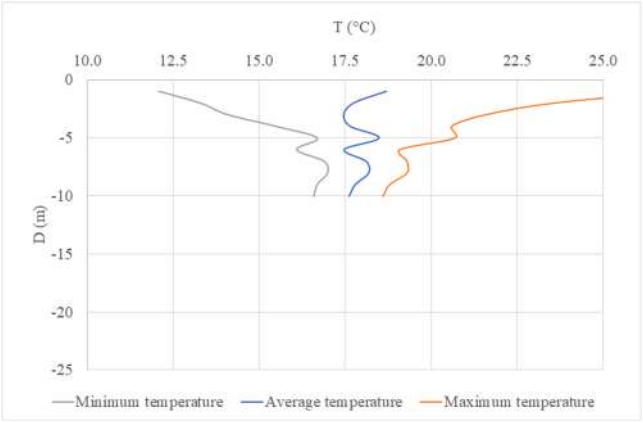

Fig. 29. Evolution of minimum, average and maximum temperature along depth for the Monitoring BHE.

configuration is particularly well suited for farms with available land and favourable shallow geothermal conditions, offering a viable pathway to reduce greenhouse gas emissions while improving energy resilience.

Future work will focus on optimising the control strategies for solar heat injection and extraction, integrating the electrical output of the PVT system into the farm energy balance, and extending the monitoring period to assess long-term thermal behaviour and sustainability over multi-year operation. These developments will further support the deployment of integrated renewable energy systems as a key component of climate-neutral livestock farming.

Funding sources

This project was funded by the European Commission, within the Horizon 2020 program for the Innovation Action project RES4LIVE "Energy Smart Livestock Farming towards Zero Fossil Fuel Consumption", running in the period 2020–2024, Grant agreement ID: 101,000,785, DOI 10.3030/101,000,785.

CRediT authorship contribution statement

Francesco Tinti: Writing – review & editing, Writing – original draft, Visualization, Validation, Software, Methodology, Investigation, Data curation, Conceptualization. **Carlos Alejandro Perez Garcia:** Formal analysis, Data curation. **Panteleimon Bakalis:** Validation, Resources. **Iván Acosta-Pazmiño:** Validation, Resources. **Stefano Benni:** Writing – review & editing, Supervision, Project administration, Methodology, Investigation, Funding acquisition, Conceptualization.

Declaration of competing interest

The authors declare that they have no known competing financial interests or personal relationships that could have appeared to influence the work reported in this paper.

Acknowledgment

The Authors want to thank the Golinelli farm, for the technical and practical assistance during the installation works over the own property.

Data availability

Data will be made available on request.

References

Alberti, L., Antelmi, M., Angelotti, A., Formentin, G., 2018. Geothermal heat pumps for sustainable farm climatization and field irrigation. Agric. Water Manag. 195, 187–200.
Asgari, N., et al., 2025. Greenhouse applications of solar photovoltaic driven heat pumps in northern environments. Renew. Sustain. Energy Rev. 207, 114920.
Barbaresi, A., et al., 2020. Application of basket geothermal heat exchangers for sustainable greenhouse cultivation. Renew. Sustain. Energy Rev. 129, 109928.
Benni, S., et al., 2023. *An integrated renewable energy plant with Smart monitoring system for sustainable farming.* IEEE International workshop on Metrology for Agriculture and Forestry (MetroAgriFor) -. Proceedings, NEW YORK, U.S.A., pp. 547–552
Benni, S., et al., 2024. In: European Conference on Precision Livestock Farming. Curran Associates, Inc., Bologna, Italy, pp. 1568–1575.
Benni, S., et al., 2025. A smart heating system based on integrated renewable energy sources for Swine nursery buildings. Energies 18 (6), 1393.
Brown, C.S., et al., 2024. Assessing the technical potential for underground thermal energy storage in the UK. Renew. Sustain. Energy Rev. 199, 114545.
Chiavetta, C., Tinti, F., Bonoli, A., 2011. Comparative life cycle assessment of renewable energy systems for heating and cooling. Procedia Eng 21, 591–597.
Deeken, H., Lengling, A., Kromweh, M., Buscher, W., 2023. Improvement of piglet rearing's energy efficiency and sustainability using air-to-air heat ex-changers—A two-year case study. Energies 16 (4), 1799.
Dhaidaan, N., et al., 2024. Enhancing the thermal performance of an agricultural solar greenhouse by geothermal energy using an earth-air heat exchanger system: a review. Geothermics 123, 103115.
Emmi, G., et al., 2017. Ground source heat pump systems in historical buildings: two Italian case studies. Energy Procedia 133, 183–194.
Fadzlin, W.A., Hasanuzzaman, M., Rahman, S.A., Said, Z., 2025. Solar thermal energy storage: global challenges, innovations, and future directions for renewable energy systems. Appl Therm Eng 280, 128346.
FAO, 2019. Livestock and Environment statistics:: Manure and Greenhouse Gas Emissions. FAO s.l.
Focaccia, S., et al., 2016. Shallow geothermal energy for industrial applications: a case study. Sustain. Energy Technol. Assess. 16, 93–105.
Ghiasi, M., Wang, Z., Mehrandezh, M., Paranjape, R., 2025. Enhancing efficiency through integration of geothermal and photovoltaic in heating systems of a greenhouse for sustainable agriculture. Sustain. Cities Soc. 118, 106040.
Giambastiani, B.M.S., Tinti, F., Mendrinos, D., Mastrocicco, M., 2014. Energy performance strategies for the large scale introduction of geothermal energy in residential and industrial buildings: the GEO.POWER project. Energy Policy 65, 315–322.
He, D., Deng, X., Wang, X., Zhang, F., 2023. Livestock greenhouse gas emission and mitigation potential in China. J. Env. Manage 348, 119494.
Hosouli, S., et al., 2023. Evaluation of a solar photovoltaic thermal (PVT) system in a dairy farm in Germany. Sol. Energy Adv. 3, 100035.
Li, J., et al., 2026. Capacity optimization of rural residential distributed photovoltaic -battery energy storage system considering uncertainties. J. Energy Storage 148, 120246.
Lombardi, G.V., Berni, R., 2021. Renewable energy in agriculture: farmers willingness-to-pay for a photovoltaic electric farm tractor. J. Clean Prod. 313, 127520.
Murali, D., et al., 2024. Experimental assessment of a solar photovoltaic-thermal system in a livestock farm in Italy. Sol. Energy Adv. 4, 100051.
Naranjo-Mendoza, C., Oyinlola, M.A., Wright, A.J., Greenough, R.M., 2019. Experimental study of a domestic solar-assisted ground source heat pump with seasonal underground thermal energy storage through shallow boreholes. Appl. Therm. Eng. 162, 114218.
Nitkiewicz, A., Sekret, R., 2014. Comparison of LCA results of low temperature heat plant using electric heat pump, absorption heat pump and gas-fired boiler. Energy Convers. Manag. 87, 647–652.
Nugrahaeningtyas, E., Lee, J.-S., Park, K.-H., 2024. Greenhouse gas emissions from livestock: sources, estimation, and mitigation. J. Anim. Sci. Technol. 66 (6), 1083–1098.
Pal, M., Dass, R., Nehra, V., 2025. Viability assessment of solar photovoltaic systems for dairy cattle farms in India. Next Res. 2, 101043.
Qamar, S.H., et al., 2026. Hybrid solar PVT systems for renewable energy in dairy farming: a performance and economic analysis in Belgium. Energy Convers. Manag.: X 29, 101555.
Ramadhani, U.H., et al., 2025. Review of solar thermal technologies in sustainable animal agriculture farms: current and potential uses. Sol. Energy 291, 113374.
Sadeghi, H., Jalali, R., Singh, R., 2024. A review of borehole thermal energy storage and its integration into district heating systems. Renew. Sustain. Energy Rev. 192, 114236.

Tamborrino, C., Biagini, L., Cacchiarelli, L., Maruejols, L., 2026. Harvests of solar light: italian agriculture in the age of the photovoltaic era. *Resources, conservation & recycling*. Issue 230, 108877.

Tiktas, A., Hepbasli, A., 2026. A key review of geothermal heat pumps: exergoeconomic and environmental aspects with prospects for further development. Next Energy 10, 100482.

Tinti, F., et al., 2022. *Investigations and modelling for a practical application of borehole thermal energy storage.* Geosciences for a Sustainable Future - Proceedings. Torino, Italy, p. 1.

Tinti, F., Tassinari, P., Rapti, D., Benni, S., 2023. Development of a pilot borehole storage system of solar thermal energy: modeling, design, and installation. Sustainability 15 (9).

Tyris, D., et al., 2022a. RES4LIVE – Energy smart livestock farming to-wards zero fossil fuel consumption. VDI Ber. 2406 (648), 493–498.

Tyris, D., et al., 2022b. RES4LIVE - Energy Smart Livestock Farming Towards Zero Fossil Fuel Consumption. VDI-Berichte s.l.

Xiuting, W., Sameti, M., Nasiri, F., Li, B., 2024. An off-grid solar district energy system with borehole thermal energy storage: life cycle assessment in a subarctic region. J. Build. Eng. 91, 109576.